Miner Petrol (2011) 101:225–244
DOI 10.1007/s00710-011-0146-x

ORIGINAL PAPER

NH_4-bearing micas in poly-metamorphic Alpujárride micaschists and gneisses from the central zone of the Betic Cordillera (Spain): tectono-metamorphic and crystal-chemical constraints

Maria Dolores Ruiz Cruz

Received: 12 October 2010 / Accepted: 1 February 2011 / Published online: 2 April 2011

Abstract The content and distribution of NH_4-bearing micas in micaschists and paragneisses of the Alpujárride complex (Betic Cordillera, Spain) are interpreted on the basis of textures, metamorphic history and crystal-chemical constraints. NH_4 is present in important amounts in early micas, recording their older diagenetic-to-metamorphic history. NH_4 was inherited by micas formed in successive metamorphic events. At similar metamorphic grade, annite is enriched in NH_4 relative to muscovite with a fractionation of 4:1. Maximum NH_4 contents were estimated in golden annite from medium-grade schists and in retrogressive annite-chlorite mixed-layers (~1.0 wt.%). A Ti-NH_4 avoidance gives rise to associated chemical changes, such as the enrichment in Mg and in ^{VI}Al. These data suggest that NH_4 can be a decisive factor in chemical equilibrium and element partitioning between coexisting phases, thus affecting to the commonly used thermobarometers. Estimation of the *P-T* conditions from texturally different muscovite-annite pairs reveals the superposition of several stages of mica growth, under different geothermal gradients.

Introduction

K-micas, muscovite (Ms) and biotite (Bt) are common rock-forming minerals in granitic and metamorphic rocks of the Earth's crust. NH_4^+ has an ionic radius slightly higher than K^+, and can also occupy the interlayer positions in the mica structure, where it coexists with variable amounts of K^+, leading to the so called ammonium micas. The NH_4 content can be, however, very variable, from the ppm to the wt.% scale. Thus, the end-member NH_4-analogue of muscovite (tobelite, Tob) has been found in nature in low- and high-temperature environments (Higashi 1982; Ruiz Cruz and Sanz de Galdeano 2008). In contrast, only one report of ammonium-rich annite (suhailite, Suh) exists at present (Ruiz Cruz and Sanz de Galdeano 2009a), although trioctahedral ammonium mica (phlogopite) has been repeatedly synthesized (Boss et al. 1988; Eugster and Muñoz 1966; Harlov et al. 2001).

According to previous data, micas from granitic rocks show ammonium contents between 10 and 100 ppm whereas these contents increase to the range of 50–500 ppm in common metamorphic micas (Hall 1988; Honma 1996; Honma and Itihara 1981; Itihara and Suwa 1985). Nevertheless, considerably higher ammonium contents (up to 3,000 ppm) have been occasionally determined in Bt from metamorphic rocks (Moine et al., 1994; Boyd and Philippot 1998; Duit et al. 1986; Visser 1992; Plessen et al., 2010).

Micas with high ammonium content are important markers of either high organic rich source rocks (Boyd and Philippot 1998; Sadofsky and Bebout 2000) or unusual N-enriched hydrothermal fluids (Hall 1988; Visser 1992). As a consequence, NH_4-mica formation is related to two main geological processes: a) N liberation during the thermal decomposition of organic matter, and fixation, as NH_4, in diagenetic clay minerals; and b) Hydrothermal alteration of pre-existing K-mica by NH_4-bearing fluids. During the first process, the NH_4:K ratio can be very variable, according to the organic matter content in or near the sediment. This process can have, in addition, a wide distribution, especially in sedimentary terrains rich in organic components, such as many Carboniferous forma-

Editorial handling: R. Abart

M. D. Ruiz Cruz (✉)
Facultad de Ciencias, Campus de Teatinos,
29071 Málaga, Spain
e-mail: mdruiz@uma.es

tions (e.g. Daniels and Altaner 1990; Williams et al., 1995; Juster et al. 1987; Nieto, 2002; Sucha et al. 1994). In the second case, NH_4 for K replacement can be extensive and almost pure NH_4-dioctahedral mica can be formed in localized geological settings (Higashi 1982).

The presence of di- and trioctahedral NH_4^+-micas (Tob and Suh) in the basement formations of the Alpujárride complex has been reported by Ruiz Cruz and Sanz de Galdeano (2008; 2009a). These micas were identified in the tectonically highest unit of this complex, the Güajares unit. Whereas relics of Tob have been found in dark micaschists through the Cordillera, Suh appears in gneisses from more restricted areas. We interpreted that Tob formed during the first diagenetic-to-metamorphic episode that affected these formations, with NH_4 derived from the maturation of organic matter, as generally accepted in the case of sedimentary terrains rich in organic components. Initially contained in Tob, NH_4 was redistributed between white mica and annite (Ann) at conditions of increasing metamorphism.

In addition to NH_4-rich micas, most gneisses and schists from the Alpujárride complex contain micas with lower and variable NH_4 contents. This manuscript deals with the important subject of ammonium in the mica minerals during metamorphism. NH_4 is not detected by the routine methods applied in metamorphic petrology, and generally overlooked. Nevertheless, other approximations can be used for estimating NH_4 in micas, such as elemental analysis of nitrogen and data derived from the basal spacing of the mica minerals. Determination of NH_4 content in mica is important because: 1) it can be used as a marker of ancient biological activity; 2) in poly-metamorphic terrains, it can provide information about the successive mica-bearing metamorphic assemblages; 3) according to previous data (Ruiz Cruz and Sanz de Galdeano 2008; 2009a; 2009b), presence of NH_4 in the interlayer can affect the composition of the octahedral sheet, thus influencing the chemical equilibrium during the metamorphic reactions and, consequently, the physical conditions deduced from the most common thermobarometers. The study of a set of selected samples, with variable metamorphic grade, will presumably help to establish the relation between the NH_4 content in micas, the metamorphic grade and the metamorphic history of these formations.

Geological setting

The Betic Cordillera has been traditionally divided into a northern external domain, the External Zone, an intermediate domain, the flysch units from the Gulf of Cádiz area, and a southern domain, the Internal Zone. The Alpine orogeny in late Cretaceous to Miocene times was accompanied by intense structural deformation and metamorphism, which particularly affected the Internal Zone. Structurally, the Internal Zone is formed of three tectonically superimposed complexes, from bottom upwards, the Nevado-Filábride, the Alpujárride and the Maláguide. The Nevado-Filábride complex, only present in the Betic zone, has been later subdivided into the Mulhacén and the Veleta complexes (Puga *et al*., 2002). The geo-tectonic relationships between the several complexes are essentially constant in the Betic Cordillera: The Maláguide complex tectonically overlies the Alpujárride complex, and this, the Nevado-Filábride complexes.

At a regional scale, the Alpujárride complex shows the superposition of rocks of different metamorphic grade belonging to various tectonic units; from bottom to top and in general order of increasing metamorphic grade (Sanz de Galdeano and López-Garrido 2003): Lújar-Escalate, Almijara, and Guájares units (Fig. 1). The lithostratigraphic sequence of the Alpujárride units is similar for the whole Alpujárride complex. It includes a metapelitic to metapsammitic sequence formed by paragneisses, dark- and light-coloured micaschists, attributed to Palaeozoic (or older) protoliths (Egeler and Simons 1969), overlain by fine-grained schists and carbonate rocks, attributed respectively to Permo-Triassic and middle and upper Triassic.

The Alpujárride rocks record, according to previous interpretations, an Alpine polyphase metamorphic history, and successive stages of deformation (D_1-D_3) and mineral growth (M_1-M_3) have been described in schists and paragneisses, based on the presence of several schistosities (S_1, S_2 (=S_p), S_c). The metamorphic climax has been interpreted as corresponding to a high pressure/low-temperature (H*P*-L*T*) eo-Alpine metamorphism (M_1), followed by nearly isothermal decompression during which the main fabric (D_2, S_2) and metamorphic assemblage (M_2) developed. The late-Alpine event 3 has been related with the development of major large-scale recumbent folds that deformed the S_2 foliation and the geometries of the metamorphic-isograds. Development of crenulation foliation (S_c) during this event was accompanied by low-pressure mineral growth (e.g. Azañón et al. 1997; Bakker et al. 1989; Balanyá et al. 1997; García-Casco and Torres-Roldán 1996; Goffé et al. 1989; Tubía and Gil-Ibarguchi 1991). The effect of the earlier Hercynian episode (Zeck and Whitehouse 1999, 2002), and of possible previous events has been, in contrast, scarcely investigated. Indeed, at present, there is no agreement about the Alpine- or pre-Alpine assignment of the metamorphic parageneses present in the basal sections of the Alpujárride units (see Zeck and Williams 2001 and references therein). Nevertheless, older metamorphic events (Hercynian and Cadomian) have been identified in other zones of the Alpine–Mediterranean mountain belts (e.g. Handler et al. 1997; Neubauer 2002).

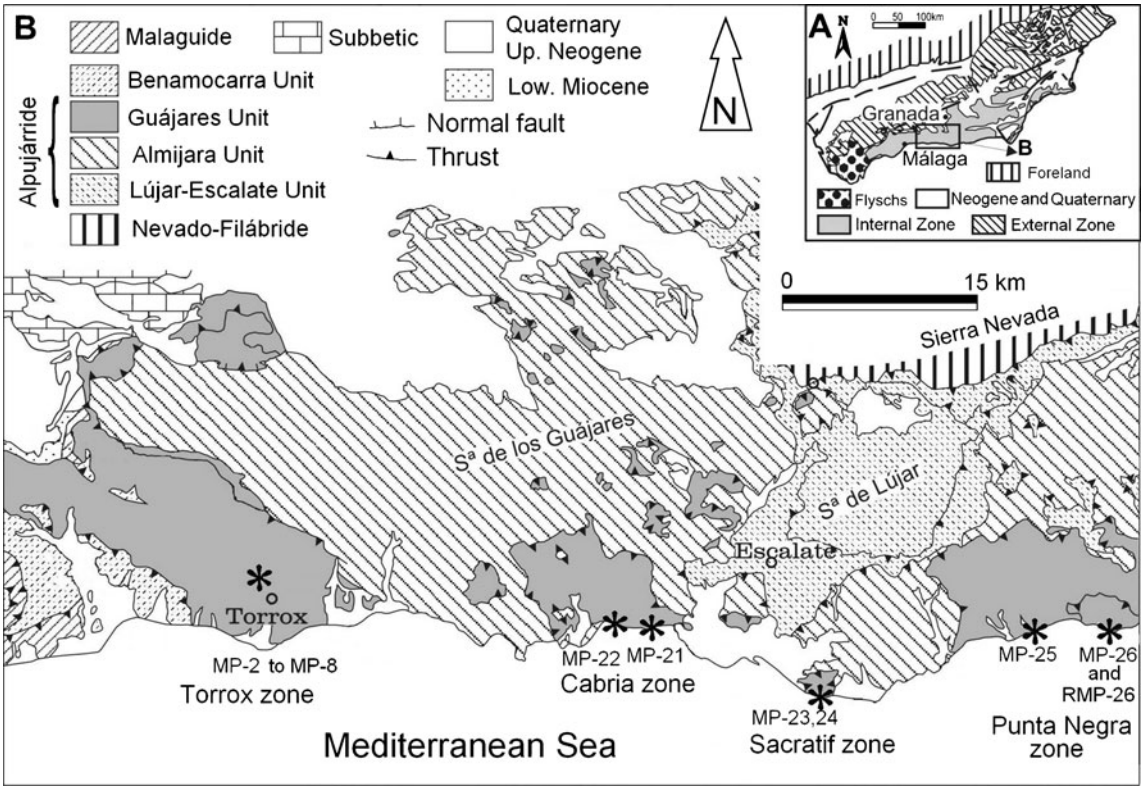

Fig. 1 Simplified geological map of the studied area, showing the position of the samples described (*stars*). Inset: Simplified tectonic map of the Betic Cordillera showing the distribution of the several Zones

Sampling and methodology

Sampling was carried out in several outcrops located between Torrox and Punta Negra (Málaga province, Spain). From a previous systematic study, some samples representative of increasing metamorphic conditions were selected for this study. Exact sample location is shown in Fig. 1 and Table 1. Samples were systematically studied by petrographic microscopy, X-ray diffraction (XRD) and Fourier transform infrared spectroscopy (FTIR). C and N determination was carried out by elemental analyses. The chemical characterization of micas was realized by electron microprobe (EMPA), X-ray energy dispersive (EDX), and analytical electron microscopy (AEM). The results presented here are mainly based on the EDX analyses since EMPA data are hindered by rapid NH_4 volatilisation, and by the presence of thin mica intergrowths and of Ti- and Fe-oxide inclusions in annite, not discernible at this scale, which lead to contaminated analyses.

XRD patterns were recorded using a Philips X'Pert PRO MPD (University of Málaga), with CuKα radiation and Ge monochromator, operated at 40 mA and 40 kV, with 0.01°2θ step size and 2 s counting time. Randomly oriented samples were used for determination of the quantitative mineral composition, using the X'Pert High Score Software package (Philips), based on Rietveld analysis, and the PDF2-2003 database (International Center for Diffraction data).

FTIR spectra were recorded in KBr pellets (2% wt. samples) using a Nicolet spectrometer (20SXB) with a DTGS detector, in the range 4,000-400 cm^{-1} (Málaga University) Resolution was 2 cm^{-1}. 400 scans were accumulated to improve the signal to noise ratio in the spectra. To avoid grinding effects in the preparation of the disk, samples and KBr were gently mixed manually. Although FTIR spectra are very useful on the NH_4 identification, their use is very limited in carbonate-bearing rocks, since carbonates show a stronger band at similar frequency than NH_4.

EMPA data were obtained with a Cameca SX100 equipment in the CIC (Granada University). EMPA analyses required a previous calibration of N using the two available standards (BN), supplied by Cameca and SPI. The beam diameter was 10 μm with accelerating voltage of 15 kV and variable beam current and counting times of N. The data were reduced using the X-PHI correction. Standards were albite (Na), periclase (Mg), synthetic SiO_2 (Si), Al_2O_3 (Al), TiO_2 (Ti), Fe_2O_3 (Fe), Cr_2O_3 (Cr), NiO (Ni), and $MnTiO_3$ (Mn), sanidine (K) and diopside (Ca).

Table 1 Location and mineral composition of the studied NH_4-bearing samples

Sample	Coordinates	Lithology	Mineralogy
MP-8	N36°45'44.3"; W4°57'23.4"	Dark, Ky-schist	Qz+Pl+Ann+Ms+Tob+Ky+Sil+And+St+Grt+(Chl)
MP-22	N36°44'43.8"-W3°39'10.1"	Dark, Ky-schist	Qz+Pl+Ann+Ms+Tob+(Ky)+Sil+And+St+Grt+(Kln)
MP-21	N36°44'39.1"-W3°37'18.8"	Ann-free, Grt-schist	Qz+Pl+Ann+Ms+Tob+(Ky)+And+St+Grt
MP-23	N36°41'43.8"-W3°28'7.9"	Ann-free Chl-schist	Qz+Pl+Ms+Prg+Chl+(Kln)
MP-24	N36°41'43.8"-W3°28'7.9"	Fine-grained Chl-quartzite	Qz+Pl+Ms+Pg+Chl
MP-25	N36°44'43.3"-W3°16'51.4"	Dark Chl-schist	Qz+Pl+Ms+Pg+Chl
MP-26	N36°44'45.4"-W3°12'42.8"	Golden Grt-schist	Qz+Pl+Ann+Ms+And+St+Grt+(Chl)
RMP-26	N36°44'45.4"-W3°12'42.8"	Golden Grt-schist	Qz+Pl+Ann+Ms+And+St+Grt+(Chl)+(ML)

Samples were studied by scanning electron microscopy (SEM), using a LEO 1430-VP scanning electron microscope (SEM), equipped with a X-ray energy dispersive (EDX) system Inca 350 (Oxford instruments), at an accelerating voltage of 20 kv and 2 nA beam current (C.I.C., Granada University). Standards were albite (Na), orthoclase (K), periclase (Mg), wollastonite (Si and Ca) and synthetic oxides (Al_2O_3, Fe_2O_3 and $MnTiO_3$).

For this work, grains of golden Ann from sample MP-26, selected from thin sections, were ion thinned for transmission-analytical electron microscopy (TEM-AEM) study. Other samples from the Torrox area were also studied by TEM-AEM in previous works. This study was carried out with a Philips CM-20 transmission electron microscope (TEM), operated at 200 kV and fitted with a scanning transmission device and solid state detector for energy-dispersion analysis (CIC, Universidad de Granada). Microanalyses were obtained in STEM mode. Quantitative determinations used the thin-film approximation of Cliff and Lorimer (1975). Albite (Na), muscovite and annite (K), albite, spessartine and muscovite (Al), forsterite and annite (Mg and Fe), spessartine (Mn) and titanite (Ca and Ti) were used as standards.

The analyses for N and C were performed with an 1,108 (Carlo Erba) CHN analyzer (University of La Coruña). Analysis conditions were: Oxidation temperature=1,020°C; reduction temperature=650°C; $P(O_2)$=100 kPa. The standard used was Sulphanilamide (BBOT). The detection limit is 0.001 wt. %. Replicate analyses indicate that the error in N determination is <0.005%. Since most mica separates only contain quartz, minor plagioclase, and chlorite as impurities, the NH_4-content in mica has been calculated assuming that the other phases are NH_4-free.

The abbreviations of minerals suggested by Whitney and Evans (2010) have been used in the text, Tables and Figures, with some additions indicated in the captions of the Figures or Tables. Ms includes muscovite and phengite.

Petrography

The samples selected for the present study are graphitous micaschists, characterized by a well-developed schistosity (S_2 or S_p) defined by the parallel orientation of phyllosilicates. The selected samples reflect, as shown below, important metamorphic gaps.

Dark schists from the westernmost part of the studied area (Torrox zone, e.g. sample MP-8) show uniform assemblages, including quartz (Qz), plagioclase (Pl), K-feldspar (Kfs), red and golden Ann (Fig. 2a and b), Ms, kyanite (Ky), sillimanite (Sil), staurolite (St), and andalusite (And). Minute atoll garnets (Grt) only persisted as inclusions in Pl, St and And. These schists will be referred as Ky-schists, although the Ky content is <5%, according to the XRD estimation. Textural data suggest that red Ann, unoriented with respect to the main schistosity S_p, formed during the first metamorphic episode, whereas golden Ann mainly grew as retrogressive transformation of red Ann. In addition to Ms, these schists contain relics of Tob, similar to that found in other areas, and described in previous papers (Ruiz Cruz and Sanz de Galdeano 2008; 2009b), also interpreted as formed during the first metamorphic episode. Moreover schists contain smaller Ann grains, included in Ky, which also pre-dates the main schistosity S_p, whereas St and And are later, post-S_p phases. Samples MP-22 and MP-21 (Cabria zone) show parageneses similar to sample MP-8, but with lower Ky contents.

Samples MP-26 and RMP-26 (1–5) (Punta Negra zone) show lower metamorphic grade, being characterized by lack of red Ann, Sil and Ky in the mineral assemblage. These samples will be referred as Grt-schists. S_1 is hardly visible in these rocks, but it seems to be defined by aligned pre-S_p Grt, which follow Qz-rich bands (Fig. 2c), deformed by S_p. Although red Ann is lacking in these samples, they contain three well-defined generations of micas, as deduced from textural relationships: A first generation consists of Ann, Ms and Ann-Ms parallel intergrowths, all included in atoll Grt (Fig. 2c and d). The second generation consists of

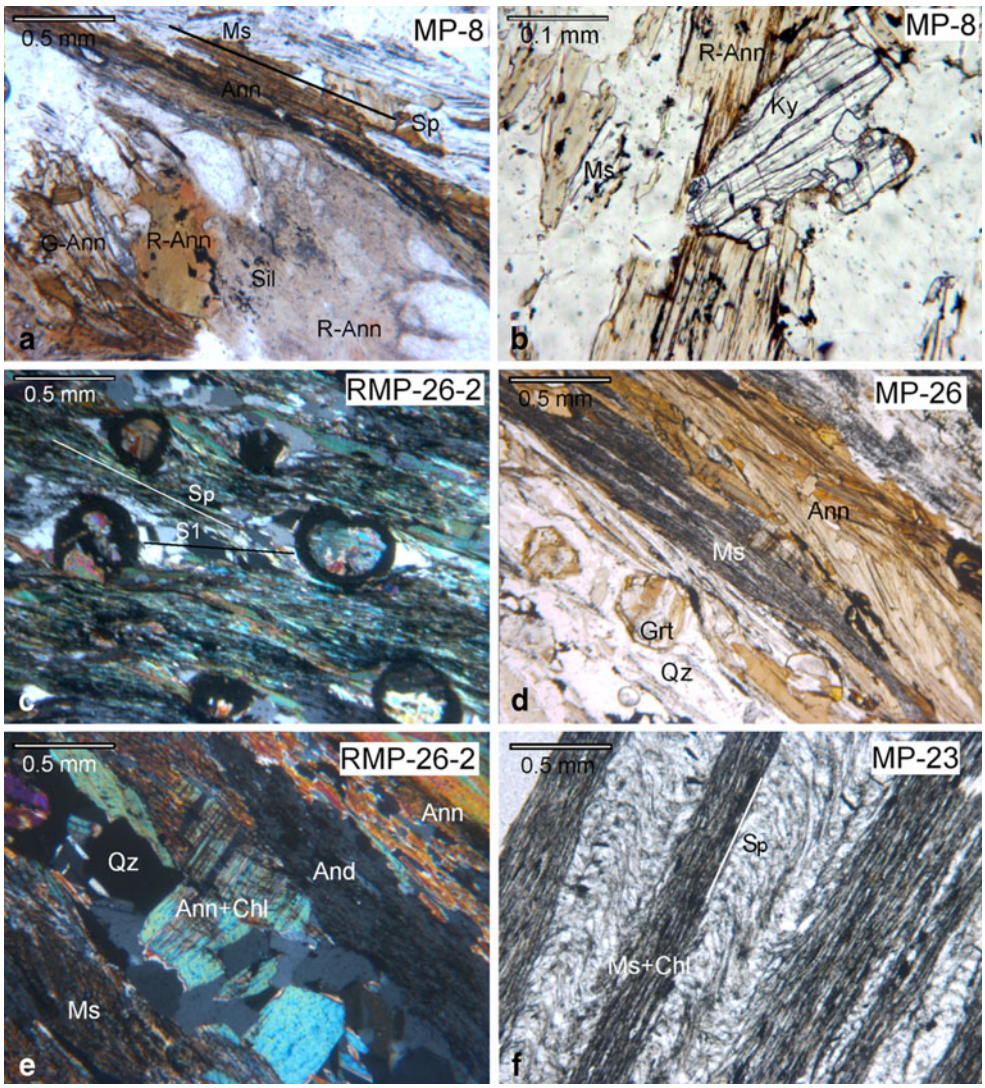

Fig. 2 Representative microscopic images of schists. **a** Red Ann-grains extensively replaced by Sil, and brown-to-golden Ann (Ky-schist MP-8, plane-polarized light). S_p is defined by G-Ann and Ms. **b** Ky grain post-dating, and partially including R-Ann (Ky-schist MP-8, plane-polarized light). **c** Schist with Qz-rich domains containing abundant atoll Grt, which define a schistosity (S_1) previous to S_p (Grt-schist RMP-26-3, crossed polars). **d** Graphite-rich Ms domains, and golden Ann domains, defining the main schistosity S_p (Grt-schist MP-26, plane-polarized light). **e** Late And grain and post-S_p intergrowths of Chl, Ann and Ann-Chl mixed-layers (Grt-schist RMP-26-2, crossed polars). **f** pre-S_p and S_p schistosities defined by Ms, Chl and Qz (Chl-schist MP-23, plane-polarized light)

alternating folia of Ms intergrown with Gr and golden Ann defining S_p (Fig. 2c and d). In addition, a third population of Ann, cross-cutting the main schistosity, appears extensively replaced by chlorite (Chl) and Ann-Chl mixed-layer minerals (ML) (Fig. 2e).

Finally, samples MP-23, MP-24 (Cabo Sacratif zone) and MP-25 (Punta Negra zone), are characterized by smaller grain-size (Fig. 2f), lack or scarcity of Ann and Grt and by the presence of the prograde assemblage Ms±Pg+Chl. These samples will be referred as Chl-schists.

The transition from Ky-bearing to Ky-free samples is characterized by important changes in mica composition and in Grt content. Three of these samples were selected for the detailed study of Grt, which provided important information about the metamorphic evolution; these results are presented in a companion paper (Ruiz Cruz 2011).

FTIR and XRD data

The presence of NH_4 in the selected samples was firstly confirmed by FTIR; most studied samples show a characteristic band in the zone of the N-H vibrations (Busigny et al. 2003; Choubari and Fripiatt 1981). Nevertheless the NH_4 content is variable according to the mica content and the dominant mica type in each sample. The N-H vibration

band appears at ~1,434 cm^{-1}, showing a shoulder at ~1,456–1,465 cm^{-1}, or, in some cases, near 1,500 cm^{-1}, in accordance with the positions observed in natural and synthetic NH_4-micas, and in Suh (Ruiz Cruz and Sanz de Galdeano 2009a). Maximum NH_4 contents are present in Ann concentrates from samples MP-8 and RMP-26, whereas the N-H vibration band is notably lower in the spectra obtained from whole-rocks. In these later spectra the presence of a weak band at 1,382 cm^{-1}, ascribed to graphite, is common. The N-H vibration band is very weak in Chl-schists (Fig. 3).

XRD data of selected whole rocks with decreasing metamorphic grade (Fig. 4a) confirm the petrographic observations, showing the prevalence of Ann in samples with the highest metamorphic grade (except for sample MP-21, where Ms is the dominant mica), Ann+Ms in samples with intermediate grade and only Ms (and occasional Pg) in samples with the lowest grade.

Since in most cases the rocks contain both Ms and Ann (e.g. MP-26 in Fig. 4a), and since the size of the mica flakes does not permit the obtaining of pure mica separates, we have manually obtained some Ms-rich and Ann-rich concentrates for the elemental analysis of N. The concentrates show variable amounts of impurities, and a quantitative determination of the mineralogical composition was carried out by XRD Rietveld-based method for estimating the mica content and the Ann:Ms ratio. According to the XRD patterns, impurities are Qz and minor Pl and Chl (Table 1, Fig. 4b). Some separates are rich in post-S_p Ann, and show important amounts of retrogressive Chl and Ann-Chl ML (sample MP-26, Fig. 4b). ML shows a very complete series of basal reflections and corresponds to a structure consisting, in average, of 2 Ann+1 Chl layers.

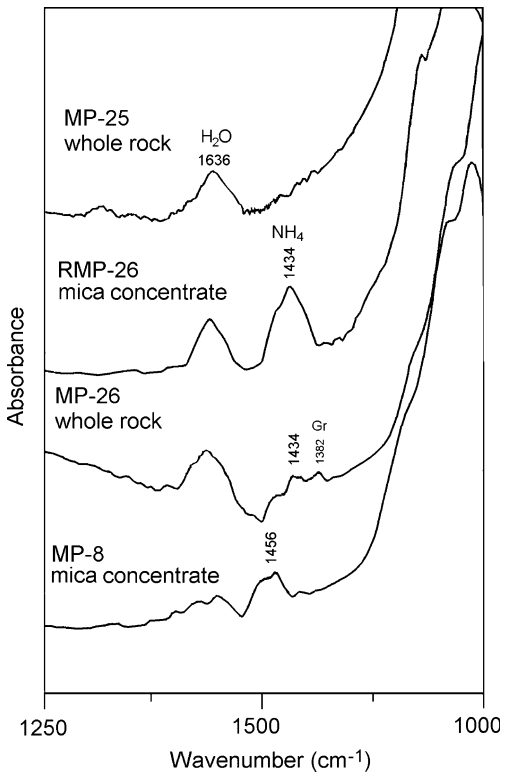

Fig. 3 FTIR spectra of samples MP-25, golden Ann concentrate from sample RMP-26, whole-rock MP-26, and red+golden Ann concentrate from sample MP-8. The N-H vibration band is very weak in sample MP-25, and, although present in all Ann-bearing samples, it increases considerably in golden Ann concentrates from sample RMP-26

XRD patterns have been also used for tentatively estimating the NH_4 content in micas, based on the exact position of the basal reflections (Fig. 4c). These patterns reveal some new features. For example, samples MP-21 and MP-22 also contain minor amounts of Tob, which was not identified during the SEM examination. In addition, the basal spacing of Ms and Ann shows important differences and permits a clear distinction between Ky- and Grt-schists. Thus, Ann from Ky-rich schists (MP-22 and MP-8) shows lower basal spacing than Ann from Ky-poorer (MP-21) and Grt-schists (MP-26 and RMP-26). These differences are evident in the zone of the 005 basal reflections (about 0.25° 2θ) and suggest that golden Ann from these later samples is enriched in NH_4 (Fig. 4c), in accordance with the FTIR data. Some authors have demonstrated that the basal spacing of illite or illite-smectite mixed-layers from diagenetic samples can be used for determining the NH_4:K ratio in the interlayer (e.g. Drits et al. 1997; 2005). Based on this evidence, and taking into account previous data for Suh with variable NH_4 contents (Ruiz Cruz and Sanz de Galdeano 2009a), the patterns in Fig. 4c would indicate that the mean NH_4 content in Ann increases from <0.07 atoms per formula unit (apfu) in samples MP-8 and MP-22 to ~0.15 apfu in sample MP-26. In contrast, Ms reflections show an inverse behaviour, suggesting that Ms from the highest grade rocks is enriched in NH_4 relative to Ms from Grt-schists. This is, however, very improbable, and the observed variations in the basal spacing of Ms must have other chemical or crystallographic explanations.

Chemical composition of micas

Selected EMPA data of the several mica populations are reported in Table 2. Since N is detectable in the analyses only when counting times are very low, the error in the determinations is high. Formulae of micas have been calculated for $O_{10}(OH)_2$, and assuming that all Fe is ferrous. This assumption is based on previous data about the Fe^{3+}/Fe^{2+} ratio determined in Suh (Ruiz Cruz and Sanz de Galdeano 2009a), and in the presence of abundant graphite in all the studied samples. Analyses of Ann and Ms with high K_2O contents (analyses 1–5, 9 and 11, in Table 2), provide formulae with interlayer occupancies near

1 atom per formula unit (apfu). Nevertheless, in analyses with lower K_2O contents (and assumed higher NH_4 contents) the interlayer occupancies are very low, suggesting an important loss of N. This is especially evident in the case of Tob analyses (analyses 12 and 13 in Table 2). Taking into account these difficulties, EDX and EMPA analyses in which N was not measured (Table 3) were used for realizing representative chemical plots (Fig. 5). Analyses corresponding to several samples have been plotted separately to favour the comparison. For sample MP-26 and similar (series RMP-26) we have also plotted separately micas included in atoll Grt and micas following the main schistosity. Similarly, for sample MP-8 we have plotted separately Ann included in Ky and syn-Sp Ann.

Analytical data indicate that Ms within the atoll Grt from samples MP-26 and series RMP-26 show rather uniform composition, with high Al, Si contents ranging from 3.00 to 3.10 apfu (Fig. 5a) and low Fe+Mg contents (Fig. 5b). Tob from schist MP-8 is clearly differentiated from the other micas in the Fe+Mg *vs.* Si diagram (Fig. 5b), where it shows notably higher Fe+Mg contents. Excluding this mica population, Ms from the other samples define two main groups: Ms from Ky-schists (MP-8 and MP-22) shows relatively restricted compositional fields, with Si content between 3.00 to 3.13 apfu, Fe+Mg contents <0.15 apfu, and low Na contents (Fig. 5c). In contrast, Ms from Ky-poorer and Grt-schists (samples MP-21, MP-26 and similar) shows wider chemical variations, with Si content up to 3.28 apfu (Fig. 5a), a phengitic trend (Fig. 5b), and higher Na contents (up to 0.37 apfu). In these latter samples (especially in sample MP-26 and RMP-26), three clusters of compositions are observed in the chemical plots, with Si content <3.07, between 3.10 and 3.13 and between 3.15 and 3.25 apfu, respectively. The high Na content (Fig. 5c) could explain the low basal spacing of Ms from these samples in relation with Ms from samples with higher metamorphic grade. Tob shows, as expected, very low Na contents. All these data, as a whole, suggest that Ms included in Grt and Tob preserve their original chemical signatures relative to secondary syn-S_p micas. In addition, the presented data suggest that Ky- and Grt-schists record different metamorphic patterns.

Ann compositions define two main trends in the ^{VI}Al vs. Si plot (Fig. 5d): A trend with a clear positive correlation (Ky-schists), and a second trend with a weaker positive correlation (sample MP-21 and Grt-schists). Ann included in atoll Gt occupies an intermediate position. Ann from the several samples defines parallel trends in the Fe+Mg vs. Si plot, without apparent relation with the metamorphic grade (Fig. 5e). In contrast, the decreasing metamorphic grade is evident in Fig. 5f, on the basis of the Ti contents. Nevertheless, whereas the trends defined by Ann from samples MP-8 and MP-22 are relatively well defined, Ann from samples MP-21 and MP-26 shows low and homogeneous Ti contents. These later contents probably reflect both lower metamorphic *T* and the higher ammonium content in these micas. Indeed, the low Ti content is a specific characteristic of NH_4-bearing Ann (Ruiz Cruz and Sanz de Galdeano 2009a). Low Ti contents also characterize Ann included in atoll Grt, probably recording a higher initial NH_4 content and a lower *T* of formation.

Considered as a whole, all these data reveal chemical trends different for Ms and Ann from Ky-schists and from Grt-schists. In addition, Ms from samples MP-8 and MP-22 shows overlapping fields, whereas Ann from these two samples shows important compositional differences, especially, in the Si and ^{VI}Al contents. This fact suggests that Ms has preserved its original signatures better than Ann.

TEM-AEM study

The TEM-AEM study was realized with the aim to structurally characterize NH_4-rich Ann from sample MP-26 and to test the true interlayer occupancy from the AEM data obtained in unaltered grains. This study showed that golden Ann is mainly composed of thick packets, where the presence of polysynthetic twining (with a mean periodicity of ~60 Å) is the most common feature (Fig. 6a). These packets do not contain Chl layers, which could be responsible for the low interlayer charge. The SAED patterns (Fig. 6a, inset) show almost continuous 0*kl* (with k≠3) reflections rows. In untwinned packets (e.g. Fig. 6b), the SAED patterns reveal, however, the presence of one-layer polytype with low stacking disorder. Isolated Chl layers were only observed in the most external parts of some Ann grains (Fig. 6b). Other areas of golden Ann show broad, damaged, lens-shaped fringes, grouped in subparallel bands of about 200–300 Å in thickness, tilted with respect to the plane (001) (Fig. 6c). This feature is more abundant in typical Suh (Ruiz Cruz and Sanz de Galdeano 2009a) and resembles the domainal microstructure described in intermediate Na-K and Na-Ca micas (Livi et al. 1997; Ruiz Cruz 2008), suggesting that NH_4-enriched Ann forms domains oblique with respect to the basal plane. Crystal defects are abundant in grains with advanced retrogression (e.g. Fig. 6d). These include variations of the basal spacing along the layers, associated to bending of layers, and presence of Ann-Chl ML areas, with mean periodicity of 34 Å, in accordance with the XRD data. The AEM data consistently yielded compositions similar to those obtained at the SEM scale, although defect-rich areas showed lower K contents, in accordance with the presence of Chl layers and ML domains.

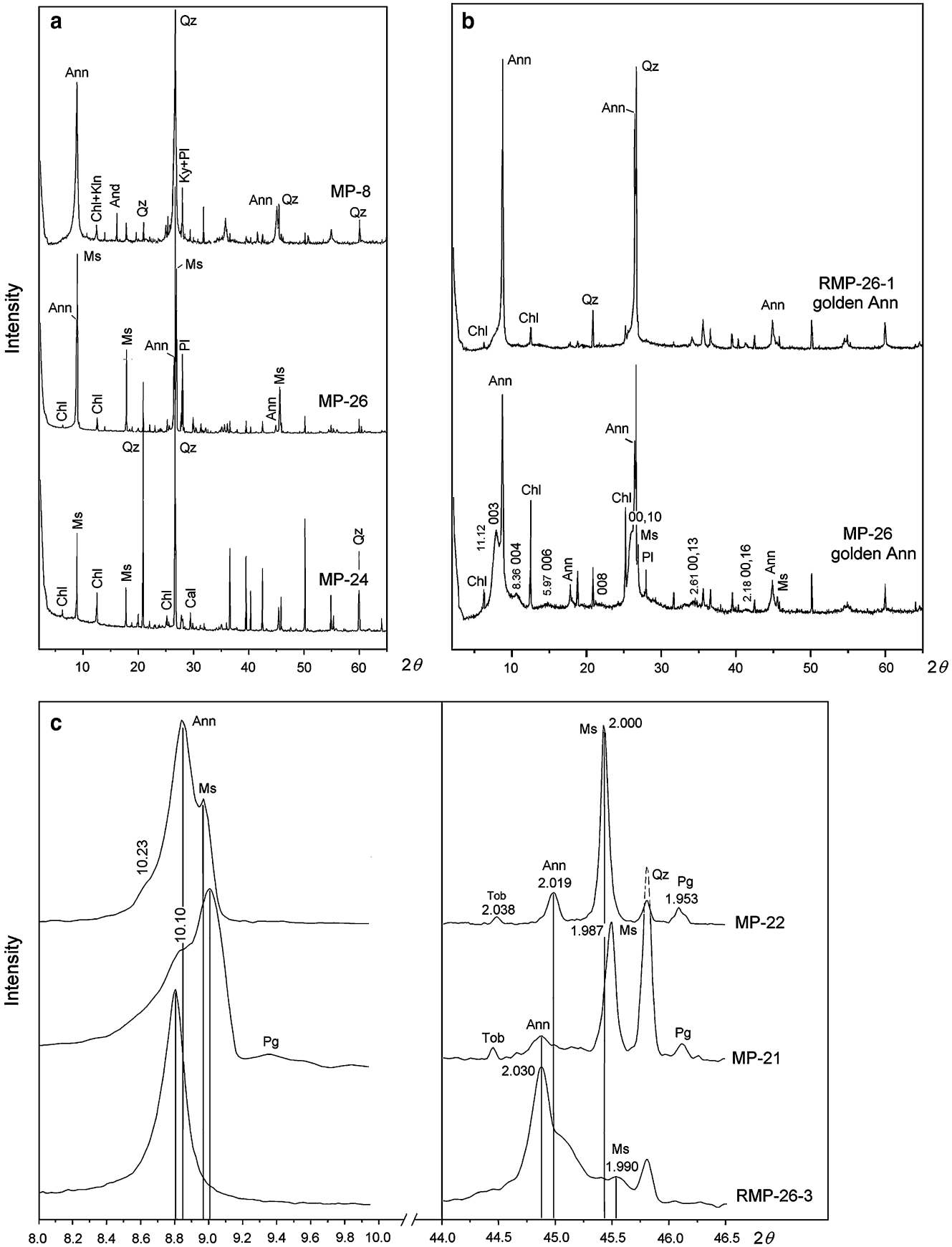
a
Qz
Ann
Chl+Kln
And
Qz
Ky+Pl
Ann
Qz
MP-8
Qz
Ms
Ms
Ann
Ms
Ann
Pl
Chl
Chl
Ms
Ann
MP-26
Qz
Qz
Ms
Qz
Chl
Chl
Ms
Chl
Cal
MP-24
Intensity
10
20
30
40
50
60
2θ
b
Ann
Qz
Ann
Chl
Qz
Ann
RMP-26-1
golden Ann
Chl
Ann
Ann
Chl
Chl
00,10
Ms
Pl
MP-26
golden Ann
11.12
003
8.36
004
5.97
006
Ann
008
2.61
00,13
2.18
00,16
Ann
Ms
Chl
10
20
30
40
50
60
2θ
c
Ann
Ms
10.23
10.10
Pg
Intensity
8.0
8.2
8.4
8.6
8.8
9.0
9.2
9.4
9.6
9.8
10.0
Ms
2.000
Ann
2.019
Qz
Pg
1.953
Tob
2.038
1.987
Ms
MP-22
Tob
Ann
Pg
MP-21
2.030
Ms
1.990
RMP-26-3
44.0
44.5
45.0
45.5
46.0
46.5
2θ

◀ **Fig. 4** **a** XRD patterns of unoriented samples with decreasing metamorphic grade (MP-8: Ky-schist; MP-26: Grt-schist; MP-24: Chl-schist). **b** XRD patterns (oriented samples) of concentrates of golden Ann from samples RMP-26-1 and MP-26. In the second pattern the basal reflections of the Ann-Chl mixed-layers have been labelled. **c** Selected zones of the XRD patterns of samples MP-22 (Ky-schist), MP-21 (Grt-schist), and RMP-26-3 (Grt-schist), showing the position of the 001 and 005 basal reflections of white micas (Ms, Tob and Pg) and Ann. Explanations see text

NH_4 contents and distribution in micas

N and C determination was carried out by elemental analysis (Schroeder and Ingall 1994; Schroeder and Mclain 1998). Table 4 shows the C and N contents determined in mica concentrates and some whole rocks. Estimation of the average NH_4 content in micas has been based on the assumption that the other phases are N-free. The possibility that a part of N be associated to graphite (Van Zuilen et al. 2005) cannot be discarded with the available data but these rather suggest that N, in the form of NH_4, is mainly present in micas. The graphite content can be estimated from the C content, since these rocks are carbonate-free. The C content ranges between 0.2 wt.% and 1.3 wt.% in the samples analyzed. Nevertheless, no correlation exists between C and N contents, the highest N contents (0.18 and 0.25 wt.%) corresponding to concentrates of golden Ann, with intermediate C contents. Moreover, the FTIR spectra (Fig. 3) show the characteristic bands of the N-H vibrations, suggesting that most N is in the form of NH_4.

Determination of the mica content was realized using Rietveld analysis and the error estimated is low; nevertheless, the content of NH_4 and $(NH_4)_2O$ (wt.%) in mica has been only calculated in mica concentrates with >50% wt. mica, and where one mica type is clearly dominant. Some analyses from gneisses of the same area, taken from Ruiz Cruz and Sanz de Galdeano (2009b) have also been included in this Table for comparison. The deduced NH_4 contents in Ms from gneisses and schists are low (0.06–0.09 wt.%) except in Grt-schists. The NH_4 content in Ann shows uniform values ranging from 0.36 in Ky-schists to 0.38 wt.% in Grt-schists. Comparison of NH_4 content in Ms- and Ann-rich concentrates indicates that Ms contains about 0.25 times as much NH_4 as Ann, which is consistent with the results of other studies of intermineral NH_4 partitioning in schists and gneisses (e.g. Boyd and Philippot 1998; Duit et al. 1986; Honma and Itihara 1981). A NH_4 enrichment in Ms and Ann was observed, however, in Grt-schists. The highest value was measured in concentrates rich in Ann-Chl ML (Fig. 4b). Estimations in this sample only can be realized assuming that the NH_4 content in Ann is similar to that determined in ML-free golden Ann concentrates from similar samples (0.38 wt. %). Hereby we deduce that the NH_4 content in the interstratified structure is about 1.0 wt.%, i.e. the Ann layers of the ML appear to be notably enriched in NH_4 relative to pure Ann.

As a whole, the NH_4 contents are higher than those typical of metamorphic rocks (Boyd and Philippot 1998; Duit et al. 1986; Mingram and Bräuer 2001). These determinations do not permit, however, an estimation of the NH_4 content in the several Ms or Ann populations from each sample. We have realized, with this aim, chemical plots (Fig. 7) showing the interlayer occupancy in the several generations of mica which, although imprecise, can help to understand the NH_4 distribution. Indeed, the NH_4 contents determined in Ms cannot result in changes detectable in the interlayer occupancies, except in Grt schists. In contrast, the $(NH_4)_2O$ contents determined in Ann concentrates (>0.50 wt.%) would correspond to about 0.1 apfu, assuming a uniform distribution of NH_4 in the whole Ann populations. The NH_4 content in the interlayer can be, however, higher if several populations of Ann with different NH_4 contents are present.

In the plot of interlayer occupancy vs. Si content (Fig. 7a), Ms from the several samples shows parallel trends of decreasing interlayer occupancy, at increasing Si contents, which could be related simply to a pyrophyllite-like substitution. Nevertheless, the lowest interlayer occupancies, probably reflecting the highest NH_4 content, are shown by phengite from sample MP-26, suggesting that increasing Si and Fe+Mg content in white mica would favour the entry of NH_4 in the interlayer, as previously suggested by Guidotti and Sassi (1998) on the basis of crystal-chemical constraints. In contrast, most Ann populations show lower interlayer occupancy (Fig. 7b); the lowest interlayer contents correspond to Ann included in Ky from the high-grade schists and to syn-S_p golden Ann from samples MP-26 and RMP-26, in accordance with the FTIR, XRD and analytical data. A high NH_4 content in Ann included in Ky is contradictory with the relatively high Ti content of this Ann, as measured at the EMPA or SEM scales (see Fig. 5f). However, the Ti content measured at the TEM scale is generally <0.10 apfu, indicating that the EDX analyses are contaminated by minute rutile (Rt) inclusions. In addition, some Ann grains from sample MP-8 (not included in Ky) also show low interlayer occupancies whereas other grains from this sample show the highest interlayer occupancies. This suggests that sample MP-8 contains several incompletely re-equilibrated Ann populations. High NH_4 contents in Ann from the Punta Negra zone (MP-26 and series RMP-26) could be tentatively related to a higher initial content in organic matter in these samples or to the lower metamorphic conditions that have affected these rocks.

Table 2 Representative chemical data (EMPA) for the several mica populations

Sample	Annite								White-micas				
	MP-8 R-Ann 1	MP-8 G-Ann 2	MP-8 In Ky 3	MP-22 R-Ann 4	MP-22 G-Ann 5	MP-26 syn-Sp 6	MP-26 syn-Sp 7	MP-26 In Grt 8	M-22 syn-Sp 9	MP-26 Syn-Sp 10	MP-26 In Grt 11	MP-8 Tob 12	MP-8 Tob 13
SiO_2	36.61	36.16	38.41	36.77	36.77	35.70	33.54	35.63	47.18	47.76	47.76	44.56	45.29
TiO_2	4.41	3.33	2.69	4.46	2.66	1.44	1.63	0.54	0.32	0.00	0.90	0.08	0.03
Al_2O_3	20.85	20.40	22.92	19.99	19.99	20.92	19.76	22.48	37.33	35.25	37.10	32.93	32.47
Cr_2O_3	0.02	0.04	0.11	0.05	0.05	0.07	0.04	0.05	0.02	0.00	0.04	0.02	0.00
NiO	0.02	0.06	0.00	0.02	0.02	0.14	0.05	0.05	0.00	0.13	0.00	0.07	0.02
MnO	0.14	0.17	0.11	0.21	0.21	0.17	0.17	0.14	0.01	0.06	0.00	0.07	0.02
FeO	18.77	22.04	17.72	20.09	20.09	19.68	18.68	17.84	1.87	0.85	1.16	7.53	7.69
MgO	7.37	6.04	4.11	6.20	6.20	7.24	7.30	8.80	0.57	0.96	0.61	2.31	2.52
CaO	0.31	0.37	0.24	0.05	0.05	0.47	0.39	0.22	0.06	1.20	0.04	1.19	1.09
Na_2O	1.05	1.13	0.58	0.43	0.43	0.96	0.93	0.18	0.77	0.38	0.66	0.33	0.35
K_2O	7.96	7.10	7.93	9.26	7.72	2.65	2.76	6.94	10.35	6.44	10.00	1.22	1.34
$(NH_4)_2O$	0.55	0.81	0.50	0.27	0.71	1.61	0.84	0.50	0.06	0.13	0.02	0.71	0.88
Cl	0.29	0.21	0.41	0.16	0.16	0.49	0.33	0.05	0.03	0.25	0.01	0.12	0.08
Total	98.05	97.64	94.29	97.81	94.90	91.05	86.09	93.30	98.53	93.03	98.29	91.02	91.70
Formulae calculated for $O_{10}(OH)_2$													
Si	2.67	2.69	2.85	2.72	2.78	2.74	2.73	2.69	3.04	3.16	3.06	3.05	3.08
^{IV}Al	1.33	1.31	1.15	1.28	1.22	1.26	1.27	1.31	0.96	0.84	0.94	0.95	0.92
^{VI}Al	0.47	0.47	0.86	0.47	0.56	0.64	0.62	0.70	1.87	1.91	1.87	1.71	1.69
Ti	0.24	0.19	0.15	0.25	0.15	0.08	0.10	0.03	0.02	0.00	0.04	0.00	0.00
Cr	0.00	0.00	0.01	0.00	0.00	0.00	0.00	0.00	0.00	0.00	0.00	0.00	0.00
Ni	0.00	0.00	0.00	0.00	0.00	0.01	0.00	0.00	0.00	0.01	0.00	0.00	0.00
Fe	1.15	1.37	1.24	1.24	1.27	1.27	1.27	1.13	0.10	0.05	0.06	0.43	0.44
Mn	0.01	0.01	0.01	0.01	0.01	0.01	0.01	0.01	0.00	0.00	0.00	0.00	0.00
Mg	0.80	0.67	0.45	0.68	0.70	0.83	0.88	0.99	0.05	0.09	0.06	0.24	0.26
∑oct	2.67	2.72	2.61	2.66	2.70	2.84	2.89	2.86	2.05	2.06	2.03	2.39	2.38
Ca	0.02	0.03	0.02	0.00	0.00	0.04	0.03	0.02	0.00	0.09	0.00	0.09	0.08
Na	0.15	0.16	0.08	0.06	0.06	0.14	0.15	0.03	0.10	0.05	0.08	0.04	0.05
K	0.74	0.67	0.75	0.87	0.74	0.26	0.29	0.67	0.85	0.54	0.82	0.11	0.12
NH_4	0.09	0.14	0.09	0.05	0.12	0.29	0.16	0.09	0.01	0.04	0.00	0.11	0.14
∑int	1.01	1.00	0.94	0.99	0.94	0.73	0.63	0.80	0.96	0.72	0.91	0.35	0.38

Discussion

The studied micaschists range in metamorphic grade from the Chl- to the Ky zone. In addition to the presence or lack of Ann, the main difference between the studied samples affects the presence of either red Ann (frequently replaced by Sil and a first generation of golden Ann) or only of syn-S_p golden Ann. A key finding for the interpretation of the metamorphic history of these schists was the presence of Ann+Ms intergrowths within atoll Grt. These mica intergrowths were previously interpreted as late replacements of Grt during Alpine exhumation in both the Torrox area and in the Alborán domain (García-Casco et al. 1993; Prosser et al. 1999). However, although late replacement textures are evident in some Grt grains, textural features, zoning patterns and electron backscattered scanning diffraction analyses clearly point to two stages of Grt growth, the first one followed by the retrogressive replacement of Grt by mica+Qz intergrowths. During the second stage the rings of atoll Grt formed (see Ruiz Cruz 2011).

Origin and evolution of NH_4-bearing micas in successive metamorphic stages

It was deduced previously (Ruiz Cruz and Sanz de Galdeano 2009b) that the first metamorphic assemblage (M_1) in the Torrox schists must have consisted of a four mica assemblage, with Tob (preserved only as scarce

Table 3 Representative chemical data (EMPA and EDX) for the several mica populations

Sample	H-Ms MP-21[1]	Sp-Ms MP-82[2]	Sp-Ms MP-83	Tob MP-84	Sp-Ms MP-225[4]	Sp-Ms MP-226[3]	Sp-Ms MP-217	Sp-Ms MP-218	AG-Ms MP-269[5]	Sp-Ms MP-2610[6]	H-Ann MP-211[1]	Suh MP-212	I-Ann MP-813	Sp-Ann MP-8142[2]	R-Ann MP-2215[3]	G-Ann MP-2216[4]	L-Ann MP-2117	AG-Ann RMP2618[5]	Sp-Ann RMP2620[6]	L-Ann RMP-2621	ML RMP-2622
SiO_2	47.67	45.12	47.01	46.58	45.26	48.04	46.93	50.16	45.81	49.02	32.79	33.50	35.87	34.79	31.93	35.94	34.76	34.72	36.25	34.67	30,52
Al_2O_3	31.84	35.27	34.04	37.43	36.09	34.61	35.18	32.14	37.32	33.21	17.96	19.66	20.19	18.71	16.12	19.22	18.26	19.39	18.11	18.39	18,53
TiO_2	1.07	1.22	0.89	0.00	0.73	0.79	0.60	0.65	0.34	0.58	4.29	0.27	3.13	3.55	3.40	2.32	1.96	1.19	1.87	1.79	1,68
FeO	1.93	1.30	1.29	5.16	1.40	1.25	1.36	1.16	1.15	1.35	23.74	26.68	20.39	23.77	28.37	20.84	23.02	23.33	22.60	24.68	27,14
MnO	0.17	0.04	0.01	0.00	0.11	0.03	0.17	0.00	0.00	0.09	0.25	0.32	0.33	0.21	0.18	0.09	0.06	0.00	0.00	0.09	0,06
MgO	1.06	0.50	0.66	3.06	0.38	0.90	0.54	1.13	0.37	1.21	5.24	7.01	5.56	5.3	5.20	7.63	6.63	7.39	7.70	7.03	8,90
CaO	0.00	0.00	0.05	1.17	0.21	0.10	0.01	0.14	0.03	0.00	0.07	0.20	0.31	0.25	0.18	0.02	0.16	0.00	0.30	0.00	0,03
Na_2O	0.41	0.27	0.41	0.29	1.37	1.30	1.01	1.46	1.92	0.69	0.09	0.12	0.13	0.15	0.58	0.33	2.91	0.44	0.66	0.00	0,00
K_2O	11.13	11.51	11.76	0.14	10.84	10.02	10.61	10.19	8.95	9.91	9.62	4.00	7.70	8.66	9.87	8.50	8.30	8.33	7.53	8.23	5,02
Total	95.28	95.23	96.12	93.83	96.38	97.05	96.42	97.04	95.89	96.08	94.05	91.76	93.61	95.39	95.83	94.88	96.06	94.78	95.02	94.88	91,87
Formulae calculated for $O_{10}(OH)_2$																					
Si	3.20	3.03	3.12	3.02	3.00	3.13	3.09	3.28	3.01	3.22	2.61	2.67	2.76	2.70	2.58	2.75	2.69	2.70	2.77	2.71	2,48
^{IV}Al	0.80	0.97	0.88	0.98	1.00	0.87	0.91	0.72	0.99	0.78	1.39	1.33	1.24	1.30	1.42	1.25	1.31	1.30	1.23	1.29	1,52
^{VI}Al	1.71	1.82	1.79	1.87	1.83	1.79	1.83	1.76	1.91	1.79	0.30	0.51	0.59	0.41	0.12	0.48	0.35	0.47	0.51	0.40	0,26
Ti	0.05	0.06	0.04	0.00	0.04	0.04	0.03	0.03	0.02	0.03	0.26	0.02	0.18	0.21	0.21	0.13	0.11	0.07	0.10	0.10	0,10
Fe	0.11	0.07	0.07	0.27	0.08	0.07	0.07	0.06	0.06	0.07	1.58	1.78	1.31	1.54	1.92	1.33	1.49	1.52	1.32	1.61	1,84
Mn	0.01	0.00	0.00	0.00	0.01	0.00	0.01	0.00	0.00	0.01	0.02	0.02	0.02	0.01	0.01	0.01	0.00	0.00	0.00	0.01	0,00
Mg	0.11	0.05	0.06	0.30	0.04	0.09	0.05	0.11	0.04	0.12	0.62	0.83	0.64	0.61	0.63	0.87	0.76	0.85	0.93	0.82	1,08
∑oct	1.99	2.01	1.97	2.45	1.98	1.99	1.99	1.96	2.02	2.01	2.78	3.18	2.74	2.78	2.88	2.82	2.72	2.91	2.86	2.95	3,29
Ca	0.00	0.00	0.00	0.08	0.01	0.01	0.00	0.01	0.00	0.00	0.01	0.03	0.03	0.02	0.02	0.00	0.01	0.00	0.00	0.00	0,00
Na	0.05	0.03	0.05	0.04	0.08	0.07	0.07	0.12	0.25	0.09	0.01	0.02	0.02	0.02	0.00	0.05	0.14	0.00	0.04	0.00	0,00
K	0.96	0.99	1.00	0.02	0.90	0.83	0.89	0.85	0.75	0.83	0.98	0.42	0.75	0.86	0.98	0.83	0.82	0.82	0.74	0.82	0,52
∑int.	1.01	1.02	1.05	0.08	0.99	0.91	0.96	0.98	1.00	0.92	1.00	0.46	0.80	0.90	1.00	0.88	0.97	0.82	0.79	0.82	0,52
XMg	0.50	0.42	0.48	0.53	0.33	0.56	0.42	0.65	0.40	0.62	0.28	0.32	0.33	0.28	0.25	0.40	0.34	0.36	0.41	0.34	0,37

H-Ms: Homogeneous (non exsolved) muscovite. Sp-Ms: Muscovite following the main schistosity. Tob: Tobelite. AG-Ms: Muscovite included in atoll-garnet

H-Ann: Homogeneous (non exsolved) annite. Suh: Suhailite. I-Ann: Annite included in kyanite. Sp-Ann: Annite following the main schistosity. R-Ann: Red annite. G-Ann: Golden Ann

AG-Ann: Annite included in atoll garnet. L-Ann: Late annite. ML: Annite-Chlorite mixed-layers (calculated for $O_{10}(OH)_2$)

Superscripts: Pairs of analyses used in projections of Fig. 9

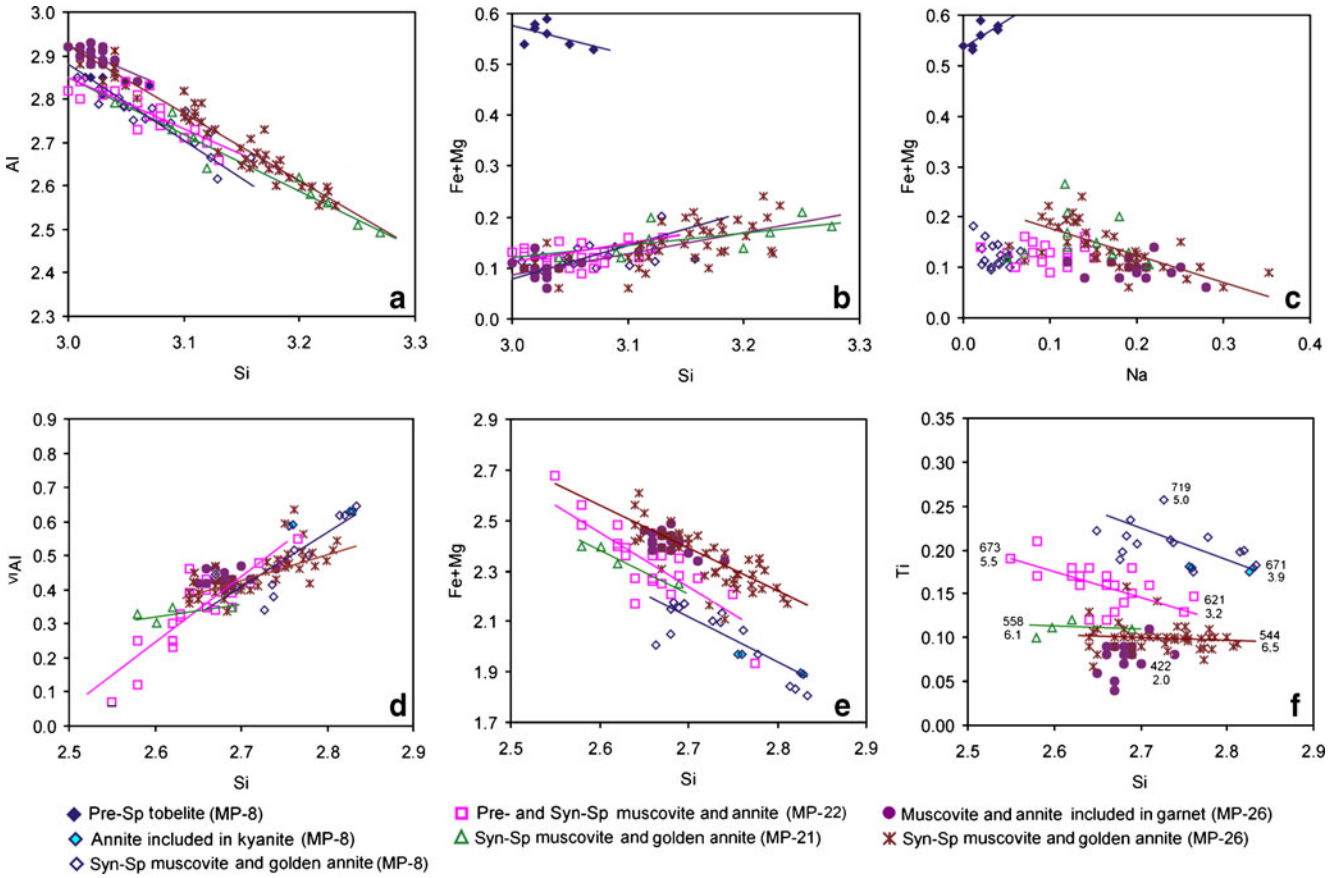

Fig. 5 Selected binary plots showing the most significant chemical characteristics of white micas **a-c** and Ann **d-f**. See text for explanation. Numbers in f indicate *T* (°C) deduced from the application of the Ti-in-Bt thermometer and *P* (kbar) deduced from the Si content in adjacent white mica

relics), Ms (also present in underlying gneisses, e.g. Fig. 8a), Ann (red annite, abundant in gneisses and locally preserved in schists, e.g. Fig. 8a, b), and NH_4-bearing Ann (mainly preserved as inclusions in Ky, e.g., Fig. 8c). This metamorphic assemblage must have formed during the first (undated) diagenetic-to-metamorphic event as a consequence of the incorporation of N derived from the organic matter in the structure of the diagenetic phyllosilicates. Data on the C content in these samples as well as the petrographic evidence of important amounts of graphite, indicate that the original protholiths contained high amounts of organic matter, reflecting important biological activity. This event could be interpreted as Hercynian (Michard et al. 1997) but numerous data rather point to a pre-Cambrian age. For example, gneisses from this area contain very characteristic intergrowths of exsolved Ms+Ann, with important amounts of NH_4 (Ruiz Cruz and Sanz de Galdeano 2009b). Detritus of these intergrowths, with preserved NH_4-mica and the same exsolution textures have been identified in Paleozoic sequences from the Maláguide Complex, unambiguously demonstrating that such formations were exposed in surface an eroded before the Silurian (Ruiz Cruz and Sanz de Galdeano 2010).

T estimated from the Ti-in-biotite thermometer (Henry et al. 2005) is >700°C and minimum *P* >7.5 kbar for gneisses, as deduced from the application of the Massone and Schreyer (1987) barometer (Fig. 9). Data derived from estimates based on core composition of Grt from Ky-schists (Fig. 8d) indicate, however, that *P* and *T* conditions probably attained 13 kbar/800°C (Ruiz Cruz submitted) during the prograde event. A first generation of golden Ann, unoriented with respect to red Ann, formed in Ky-schists as a consequence of the replacement of red Ann by Sil (Foster 1990), during the subsequent retrogressive stage (Figs. 8b and 9). This first metamorphic event (not identified previously) appears to be responsible for the important gaps in metamorphic grade observed in this area. As a consequence, micas formed during this event are only recognized in high-grade schists. As a whole, Ann from Ky-schists contain important amounts of NH_4 (0.36 wt.%), which appear to be concentrated in the golden retrogressive grains. This means that NH_4 persisted in the mica structure

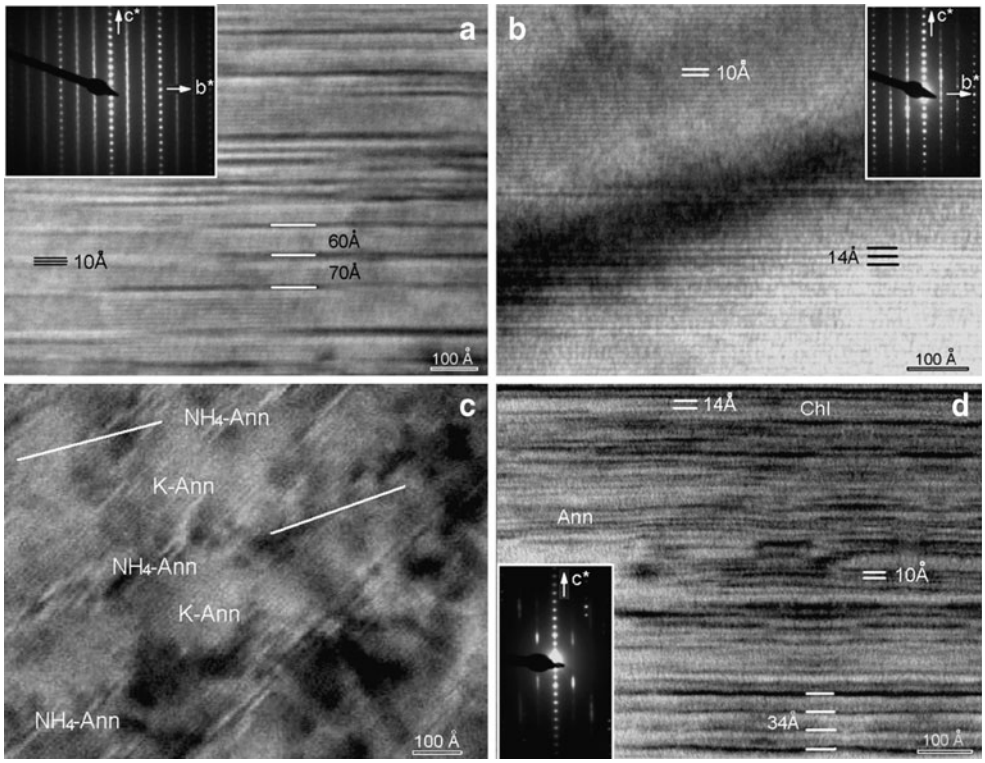

Fig. 6 Lattice-fringe images of golden Ann from sample MP-26. **a** Unaltered Ann grain with polysynthetic twinning. Presence of semi-periodic twinning originates in the SAED pattern (inset) higher-order reflections in the *hkl* reflection rows with $k \neq 3n$. **b** Beginning of the retrogression to Chl in the most external part of an Ann grain. The SAED pattern (inset) corresponds to one-layer polytype. **c** Lattice-fringe image showing sub-parallel bands, oblique to (001), of mica domains with uniform periodicity and mica domains with light broad fringes, interpreted as corresponding, respectively, to K-rich Ann and NH_4-rich Ann domains. **d** Areas of golden Ann grains with advanced retrogression. These areas show abundant crystalline defects and domains of Ann-Chl ML with mean periodicity of 34 Å. Although these domains are not abundant in the shown area, the SAED pattern (inset) shows some stretching parallel to c* of the basal reflections

at *T* higher than generally assumed. This first metamorphic episode was certainly pre-Alpine, but the precise age is yet uncertain. So far, isotopic dating of these micas have not been carried out, but the extremely fast rock uplifts and concomitant cooling rates, which characterize the extensional stage (Neogene) of the Alpine orogeny, make it difficult to deduce the age of this old stage of mica growth. Indeed, very precise ages (19-20 Ma) have been obtained from $^{40}Ar/^{39}Ar$ data on Amp, Ms, Bt and Kfs from different tectono-metamorphic units of the Western Alpujarrides (e.g. Monié et al. 1994) for the rapid rock uplift/cooling, but this event has hidden the earlier history of these rocks.

A second metamorphic event (M_2) is clearly defined by the first stage of growth of atoll Grt in medium-grade schists. Thermobarometric data deduced from the Grt study (Ruiz Cruz 2011), indicate that Grt formed at relatively high *P* (9-10 kbar) and maximal *T* on the order of 550°C. Nevertheless, the relationships between the first mica generation described before and the stage of atoll Grt growth are uncertain since, in Ky-bearing schists, atoll Grt has been mainly preserved as rare inclusions in Pl and And. This second event could tentatively be related to the first H*P*-L*T* eo-Alpine episode. Micas formed during this event have not been identified. Indeed, Ms-Ann intergrowths pervasively replaced Grt during a subsequent retrogressive stage (Fig. 8e). Although perhaps re-equilibrated to some extent during the growth of the Grt rings, Ms and Ann intergrowths preserve some of their initial chemical signatures (Fig. 5). A characteristic feature is the low Si content in Ms, suggesting low *P* of formation, and the low Ti content of Ann, defining a low-*P* retrogressive path in the *P*-*T* space (Fig. 9). We have not precise data about the NH_4 content of this Ann population, except those supplied by the interlayer charge (Fig. 7b), which suggests intermediate NH_4 contents.

The second episode of Grt growth in medium-grade schists originated the Grt rings (Fig. 8e). Thermobarometric data (Ruiz Cruz 2011) indicate for Grt rings lower *P* (5–7 kbar) and higher *T* (550–580°C) than for the core, revealing that rings grew during a subsequent and independent metamorphic event (M_3). Micas defining the main schistosity must have formed either contemporarily with Grt rings or during a later stage. These micas have been previously interpreted as formed during exhumation (Monié

Table 4 C and N contents and deduced NH_4 and $(NH_4)_2O$ contents in micas

	C	N	Mica[a]	Ms+Pg	Ann	ML	Ann NH_4	Ann $(NH_4)_2O$	ML NH_4	ML $(NH_4)_2O$	Ms NH_4	Ms $(NH_4)_2O$
Gneisses												
MP-2 (Red-Ann concentrate)	0.713	0.043	25	5	20							
MP-3 (Ms concentrate)	0.182	0.056	80	75	5						0.09	0.13
MP-4 (Ms concentrate)	0.772	0.054	93	80	13						0.07	0.10
MP-6 (whole rock)	0.431	0.065	40	5	35							
Schists												
MP-8 (Red+Golden Ann concentrate)	0.801	0.089	50	5	32		0.36	0.52				
MP-22 (Red-Ann concentrate)	1.299	0.052	42	8	34							
MP-21 (whole rock)	0.302	0.029	41	32	9							
MP-23 (whole rock)	0.248	0.028	28	28								
MP-24 (whole rock)	0.383	0.021	35	35								
MP-25 (Ms concentrate)	0.857	0.036	74	74							0.06	0.09
MP-26 (Ms concentrate)	0.936	0.067	63	55	8						0.16	0.23
MP-26 (Golden-Ann concentrate)	0.783	0.245	62	2	30	30	0.38[b]	0.55	1.00	1.45		
RMP-26-3 (Golden-Ann concentrate)	0.539	0.177	63	3	60		0.38	0.55				

All values in wt.%

Mica[a]: Mica content and composition estimated from the XRD patterns

[b] Assumed

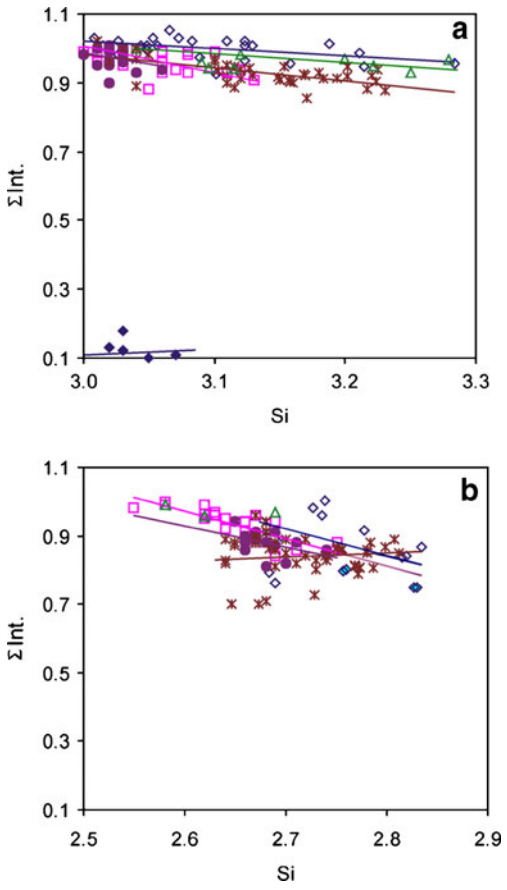

Fig. 7 Interlayer occupancy vs. Si content (apfu) in Ms **a** and Ann **b** from several samples. Symbols as in Fig. 5

et al. 1994; Platt and Vissers 1989; Platt et al. 1998; Vissers et al. 1995; Zeck 1996). Nevertheless, the chemical signatures of some of these micas (e.g. the phengitic trend observed in Fig. 5b for white micas from Grt-schists) strongly suggest that most of these micas grew during a prograde event, probably overlapping the last stage of Grt growth. This event has been unambiguously identified in Alpujárride formations from other zones, based on the presence of pumpellyite-bearing assemblages and on the chemical evolution of zoned amphiboles (Ruiz Cruz 2010; Ruiz Cruz et al. 2010). Syn-S_p micas define two parallel trends in the *P-T* space (Fig. 9): a first trend is defined by Ms with Si contents between 3.10 and 3.13 apfu, which could represent partially re-equilibrated micas. The second trend corresponds to higher-*P* Ms (phengite) and seems to define the main stage of golden Ann+Ms growth. Syn-S_p golden Ann contains important amounts of NH_4, clearly indicating that NH_4 was incorporated in the later generation of Ann. The retrogressive stage (M_4) is mainly characterized by growth of large And porphyroblasts and by retrogression of golden Ann to Chl and Ann-Chl ML (Fig. 2f), which are also characterized by high NH_4 contents.

Although an approximate estimation of the *P-T* conditions of mica growth (based on the Ti content in Ann and on the Si content in Ms) is indicated in Fig. 9, more accurate thermobarometric estimates, mainly based on Grt-bearing assemblages, are reported in a companion paper (Ruiz Cruz 2011), and schematically reported in Fig. 9 (inset).

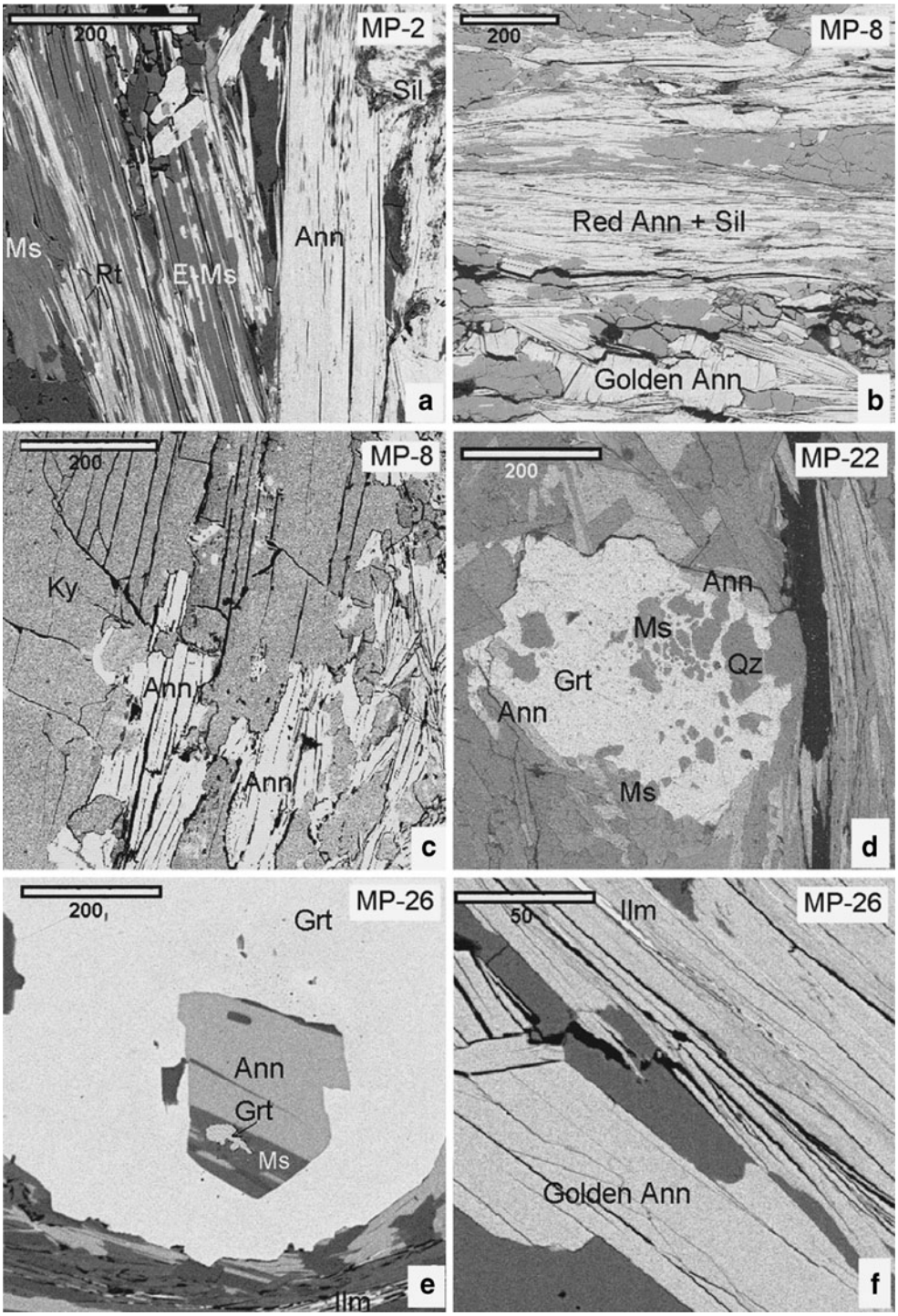

Fig. 8 Representative back-scattered electron images of micas formed in successive metamorphic stages. **a** Homogeneous Ms (Ms), exsolved Ms (E-Ms) and homogeneous red Ann extensively replaced by Sil (gneiss MP-2). This assemblage is interpreted as representative of the first prograde and retrogressive pre-Alpine metamorphic event. **b** Red Ann extensively replaced by Sil and golden Ann, interpreted as formed during retrogression of the first metamorphic event (sample MP-8). **c** Small grains of Ann, included in Ky grains (sample MP-8). **d** In sample MP-22 Grt includes abundant Qz and Ms, and minor Ann grains. **e** Ms+Ann intergrowths formed from retrogression of the first Grt generation in sample MP-26. Note the presence of Grt islands and that mica intergrowths preserve the original morphology of Grt. The second Grt generation overgrowths the Ms+Ann intergrowths and is interpreted as formed during a later high-*P* metamorphic event. Note the presence of Ilm grains intergrown with golden Ann defining the main schistosity. f: Golden Ann domain from sample MP-26, interpreted as formed during a later prograde episode. Ann is intergrown with Ilm

Factors controlling the NH_4 content in micas

It has been postulated that the NH_4 content in micas varies inversely to the metamorphic grade, as shown, e.g., by Duit et al. (1986) who studied micas from metapelites at grades ranging from the Bt zone to high-grade migmatites and granites. They recorded NH_4 only at trace levels for Ms and Bt, but the average values decreased as a function of grade, from 500 ppm to 120 ppm for Ms, and 1,500 to 300 ppm for Bt. The data presented here suggest that the NH_4 contents in micas is mainly dependent on the NH_4 availability at the time of mica growth. Data in Table 4 indicate that mean NH_4 contents in Ann from schists with variable metamorphic grade is very similar (0.36 wt.% in Ky-schists, and 0.38 wt.% in Grt-schists). The NH_4 contents in Ms are more variable (0.06–0.16 wt.%), suggesting that this content is dependent of the organic mater content and of

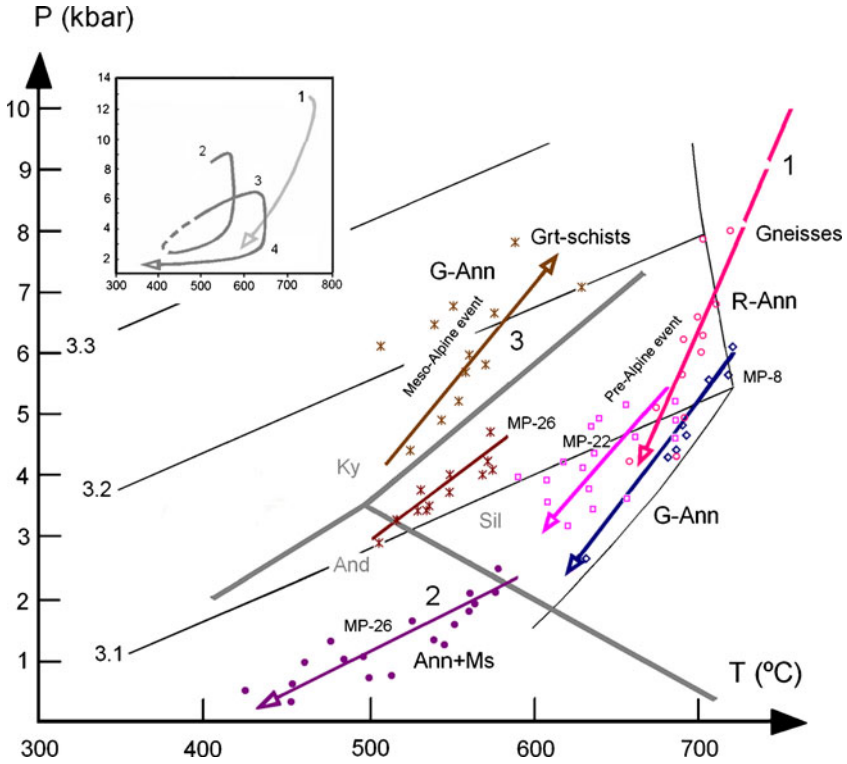

Fig. 9 *P-T* paths defined by the several mica generations, based on the Ti content in Ann (Henry et *al.*, 2005) and Si content in Ms (Massone & Schreyer, 1987) from numerous pairs Ann-Ms. Symbols as in Fig. 5. Paht 1 corresponds to retrogression of red-to-golden Ann, as observed in gneisses and Ky-schists shown in Figs. 2a, Figs. 8a and b. Path 2 corresponds to Ann +Ms intergrowths formed from retrogression of Grt, as observed in Figs. 2c, d and 8e. Path 3 corresponds to syn-Sp micas from Grt-schists, as observed in Figs. 2c-e and 8f. The phengitic trend defined by these white micas in Fig. 5b suggests that these micas mainly grew during a prograde event. Inset: Schematic *P-T* paths for successive metamorphic episodes identified in the rocks studied, as deduced from data in Ruiz Cruz (2011)

the presence of other phases (e.g. Ann) with capacity for lodging ammonium. The local increase in NH_4 observed in some Grt-schists, appears to be related to the presence of post-S_2 Ann-Chl ML, suggesting the influence of crystal-chemical constraints.

The possibility of a crystal-chemical control of the NH_4 content in Ann can be analyzed on the basis of the chemical variations observed in the several Ann populations. The main differences between the chemical trends defined by Ann with variable NH_4 contents are well observed in the plots of Fig. 10. The interlayer occupancy shows a negative correlation with ^{VI}Al in Ann from all samples, although this correlation is less clear in Grt-schists. In all samples, negative correlations between the interlayer occupancy and X_{Mg} are observed (Fig. 10b), whereas a positive correlation between interlayer occupancy and Ti for was recorded by the Ky-schists (Fig. 10c). Ann from sample MP-26, with very low Ti contents does not show a defined trend. Similar relationships had been previously described in Ann (e.g. Guidotti 1984) and explained through the coupled $Fe_1^{2+}Mg_{-1}$, $Mg_1Si_1{}^{VI}Al_{-1}{}^{IV}Al_{-1}$ and $Mg_1Si_1{}^{VI}Ti_{-1}{}^{IV}Al_{-2}$ vectors. However, in Ky-schists, ^{IV}Al and Ti show a clear positive correlation (Fig. 5f), suggesting the contribution of the $Mg_1Si_1{}^{VI}Ti_{-1}{}^{IV}Al_{-2}$ substitution. In contrast, in the NH_4-richer Ann from Grt-schists (Fig. 5f), ^{IV}Al and Ti show no correlation, suggesting that Si (or ^{IV}Al) is not involved in the substitutions leading to the impoverishment in Ti. Chemical formulae suggest that the main vectors associated to increasing amounts of NH_4 are $Mg_2^{2+}\square Ti_{-1}^{4+}$ and $^{VI}Al_4^{3+}\square Ti_{-3}^{4+}$ as evident from plotting Ti vs. Mg and ^{VI}Al (Fig. 10d and e). Clearly, these substitutions are associated with the parallel decrease of octahedral vacancies.

The decrease of Ti content in NH_4-rich Ann from gneisses has been related to exsolution of Rt during the red Ann-to golden Ann transformation, which remains as inclusions in Ann (Ruiz Cruz and Sanz de Galdeano 2009b) (Fig. 8a). In schists with lower metamorphic grade Rt is lacking but Ilm is commonly intergrown with golden Ann (Fig. 8d and f), suggesting that available Ti and Fe were only partially incorporated in the structure of the NH_4-rich golden Ann, causing the parallel enrichment in both ^{VI}Al and Mg. This indicates, however, that the compositional changes are not the cause of the NH_4 incorporation, but caused by the entry of NH_4 in the interlayer. Why the entry of NH_4 in the interlayer hinders the entry of Ti in the octahedral sheet, leading to a series of associated chemical changes is not clear, however. Structural changes caused by Ti incorporation in the octahedral sheet of Bt with variable composition have been studied in natural and synthetic Bt, and the main vectors causing the entry of Ti have been tested (e.g. Abrecht and Hewitt 1988; Brigatti et al. 1991; Hewitt and Abrecht 1986). The evident fractionation of NH_4 into Bt vs. Ms is due to the larger XII site in Bt, which would

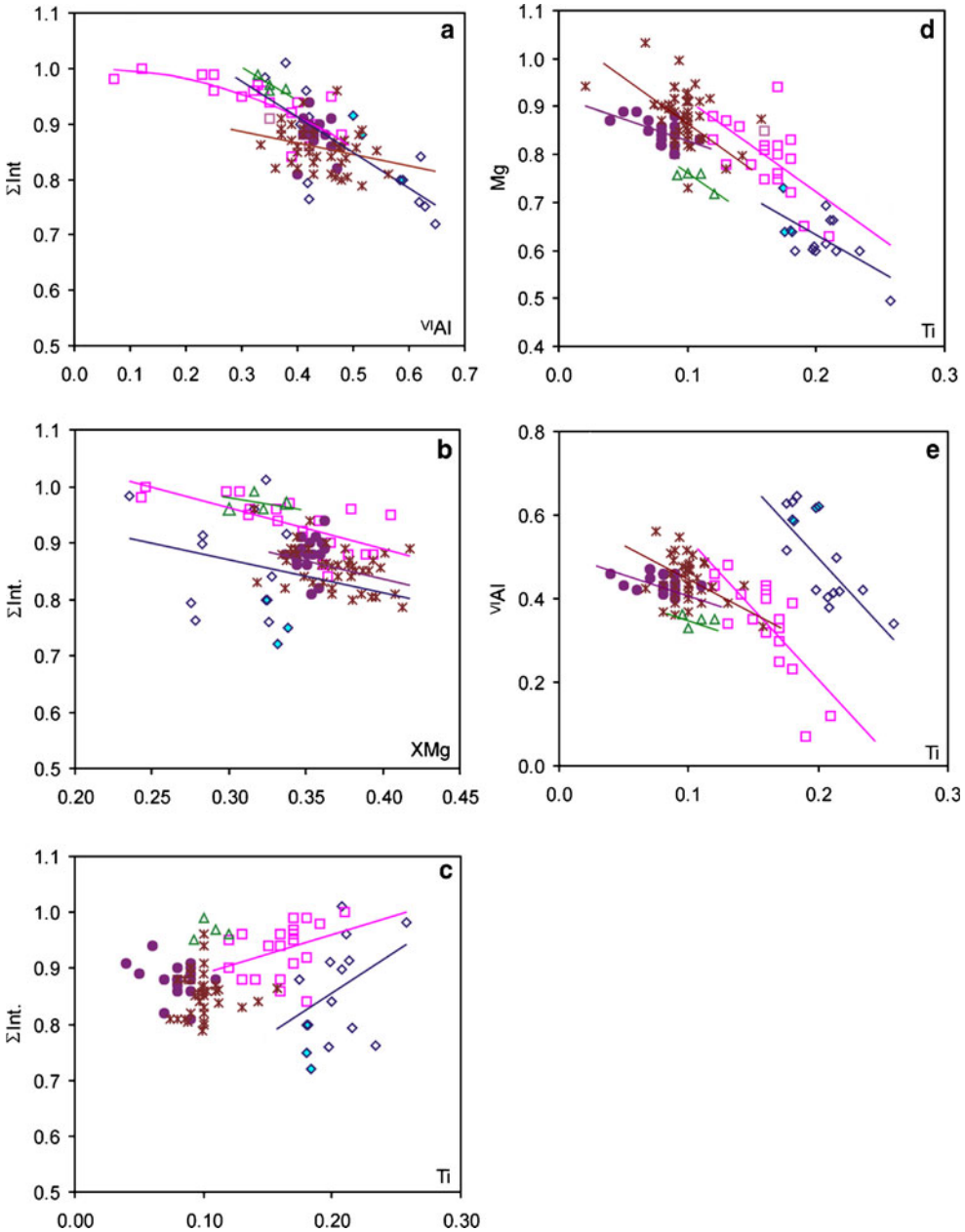

Fig. 10 Selected binary plots showing the most significant chemical variations associated to the increase of NH_4 (a-c) and the associated decrease of Ti (c and d) in Ann

more easily accommodate the larger NH_4^+ ion. It is possible that decreasing amounts of Ti in the octahedral sheet, when it is associated with the loss of vacancies, has a similar effect, *i.e.*, the increasing size of the interlayer sites, which could explain the observed Ti-NH_4 avoidance.

The fractionation of NH_4 into Ann-Chl ML vs. Ann is another curious behaviour, in clear disagreement with previous observations (e.g. Sadofsky and Bebout 2000), which indicated that retrogression of Bt to Chl is accompanied by loss of NH_4, related to fluid ↔ mineral N exchange. The behaviour observed reflects, in contrast, selective loss of K^+ during chloritization, which was perhaps controlled by hydration energy (Teppen and Miller 2006) rather than by simple relative cation concentration, as determined by the laws of mass action. Another possible explanation is that Ann layers in the ML structure contain vacancies in the A-site, caused during the Ann-to-Chl transformation. Presence of vacancies could result in weaker cohesion between layers, so favouring the entry of NH_4 in these structures.

Conclusions

As suggested in previous works, NH_4-bearing white mica and Ann are widespread in the basement formations of the Alpujárride complex, revealing that these formations, rich in organic matter, were deposited during a period of high

biological activity. NH_4-bearing micas appear to be stable phases even at T>700°C. The wide distribution of NH_4-mica in the units studied suggests that NH_4-mica can also be widespread in basement formations with similar age from other Internal-Zone complexes of the Betic-Rif orogen.

NH_4-bearing micas form a part of successive (pre-Alpine and Alpine) metamorphic parageneses, which had not been previously identified, indicating that during the several stages of mica growth, NH_4 was not lost, but incorporated in the newly formed micas. A clear enrichment in NH_4 was observed in retrogressive Ann-Chl ML from Grt-schists, indicating that during the fluid-rock interactions K was preferentially lost relative to NH_4. Nevertheless, in schists with the lowest metamorphic grade (Chl-schists), the NH_4 content in whole-rocks decreases, probably reflecting lack of Ann in these samples, since the C content of some of these samples also indicates high initial contents in organic matter.

Ammonium-bearing Ms (with maximal NH_4 contents on the order of 0.15 wt.%), is characterized by a clear phengitic trend (Fe+Mg contents varying between 0.10 and 0.25 apfu), coupled with decreasing amounts of Na (from 0.25 to 0.10 apfu), at increasing phengitic substitution. As compared with typical Tob from this area, it is evident that both white mica populations show different chemical trends, indicating the presence of a miscibility gap.

Ammonium-bearing Ann shows some clear chemical trends, at increasing NH_4 contents, which include: increase of ^{VI}Al (>0.4 apfu for 11 oxygens), and Mg contents (>0.8 apfu), and decrease of the Ti content (<0.15 apfu). Differences in chemical compositions are mainly controlled by the entry of NH_4 in the interlayer, which prevents the entry of the available Ti.

In summary, the NH_4 content of Ms might be of concern only in situations involving very low metamorphic grades and the presence of large amounts of organic material, especially if there are indications that the rocks were deposited in highly reducing or anoxic conditions, in accordance with Guidotti and Sassi (1998). Nevertheless, NH_4 contents of Ann could be of concern, as one of the commonly overlooked, but potentially petrologically important cations, since the associated chemical modifications notably influence the relative content of cations commonly used for defining chemical equilibria and for calibrating the corresponding geothermometers.

Acknowledgements The author is grateful to M. Okrusch for its excellent editorial work; to B. Mingram-Plessen and E. Puga for the careful revision of the manuscript and their constructive comments. To C. Sanz de Galdeano for help in field work and for the discussion of the results; to M.M. Abad for help in obtaining TEM–AEM data; and to M. Bentabol for the FTIR spectra. This study has received financial support from the Project CGL 2009-08186 (Ministerio de Ciencia e Innovación) and from the Research Group RNM–199 (Junta de Andalucía).

References

Abrecht J, Hewitt DA (1988) Experimental evidence on the substitution of Ti in biotite. Am Mineral 73:1275–1284

Azañón J, Crespo-Blanc, García-Dueñas V (1997) Continental collision, crustal thinning and nappe forming during the pre-Miocene evolution of the Alpujárride Complex (Alboran Domain, Betics). J Struct Geol 19:1055–1071

Bakker HE, De Jong K, Helmers H, Biermann C (1989) The geodynamic evolution of the Internal Zone of the Betic Cordilleras (South-East Spain): a model based on structural analysis and geothermobarometry. J Metam Geol 7:359–381

Balanyá JC, García-Dueñas V, Azañón JM, Sánchez-Gómez M (1997) Alternating contractional and extensional events in the Alpujarride nappes of the Alboran Domain (Betics, Gibraltar Arc). Tectonics 16:226–238

Boss A, Duit W, van der Eerde AJ, Jansen JB (1988) Nitrogen storage in biotite: an experimental study of the ammonium and potassium partitioning between 1 M phlogopite and vapour at 2 kb. Geochim Cosmochim Acta 52:1275–1283

Boyd R, Philippot P (1998) Precambrian ammonium biogeochemistry: a study of the Moine metasediments. Chem Geol 144:257–268

Brigatti MF, Galli E, Poppi L (1991) Effect of Ti substitution in biotite-1 M crystal chemistry. Am Miner 76:1174–1183

Busigny V, Cartigny P, Philippot P, Javoy M (2003) Ammonium quantification in muscovite by infrared spectroscopy. Chem Geol 198:21–31

Choubari B, Fripiatt JJ (1981) Determination of tetrahedral substitution and interlayer surface heterogeneity from vibrational spectra of ammonium in smectites. Clays Clay Miner 29:260–268

Cliff G, Lorimer GW (1975) The quantitative analysis of thin specimens. J Micros 103:203–207

Daniels EJ, Altaner SP (1990) Clay mineral authigenesis in coal and shale from the Anthracite region, Pennsylvania. Am Miner 75:825–839

Drits VA, Lindgreen H, Salyn AL (1997) Determination of the content and distribution of fixed ammonium in Illite-smectite by X-ray diffraction: application to North See Illite-smectite. Am Miner 82:79–87

Drits VA, Sakharov BA, AlL S, Lindgreenm H (2005) Determination of the content and distribution of fixed ammonium in illite-smectite using a modified X-ray diffraction technique: application to oil source rocks of western Greenland. Am Miner 90:71–84

Duit W, Jansen JH, Van Breemen A, Bos A (1986) Ammonium micas in metamorphic rocks as exemplified by Dôme de l'Agot (France). Am J Sci 286:702–732

Egeler G, Simon OJ (1969) Orogenic evolution of the Betic Zone (Betic Cordilleras, Spain), with emphasis on the nappe structures. Geol Mijnb 48:296–305

Eugster HP, Muñoz J (1966) Ammonium micas: possible sources of atmospheric ammonia and nitrogen. Science 151:683–686

Foster CT (1990) The role of biotite as a catalyst in reaction mechanisms that form fibrolite. Geol Mineral Assoc Canada 15:A40

García-Casco A, Torres-Roldán R (1996) Disequilibrium induced by fast decompression in St–Bt–Grt–Ky–Sil–And metapelites from the Betic Belt (Southern Spain). J Petrol 37:1207–1239

García-Casco A, Sánchez-Navas A, Torres-Roldán RL (1993) Disequilibrium decomposition and breakdown of muscovite in high P-T gneisses, Betic alpine belt (southern Spain). Am Miner 78:158–177

Goffé B, Michard A, García-Dueñas V, González-Lodeiro F, Monié P, Campos J, Galindo-Zaldívar J, Jabaloy A, Martínez-Martínez JM, Simancas F (1989) First evidence of high pressure, low temperature metamorphism in the Alpujarride nappes, Betic Cordilleras (SE Spain). Eur J Mineral 1:139–142

Guidotti CV (1984) Micas in metamorphic rocks. Rev Mineral 13:357–467

Guidotti CV, Sassi FP (1998) Petrogenetic significance of Na-K white mica mineralogy: recent advances for metamorphic rocks. Eur J Mineral 19:815–854

Hall A (1988) The distribution of ammonium in granites from Southwest England. J Geol Soc 145:37–41

Handler R, Dallmeyer RD, Neubauer F (1997) $^{40}Ar/^{39}Ar$ ages of detrital white mica from Upper Austroalpine units in the Eastern Alps, Austria: evidence for Cadomian and contrasting Variscan sources. Geol Runds 86:69–80

Harlov DE, Andrut M, Melzer S (2001) Characterization of NH_4-phlogopite $(NH_4)(Mg_3)[AlSi_3O_{10}](OH)_2$ and ND_4-phlogopite $(ND_4)(Mg_3)[AlSi_3O_{10}](OD)_2$ using IR spectroscopy and Rietveld refinement of XRD spectra. Phys Chem Miner 28:77–86

Henry DJ, Guidotti CV, Thomson JA (2005) The Ti-saturation surface for low-to-medium pressure metapelitic biotite: Implications for geothermometry and Ti-substitution mechanisms. Am Miner 90:316–328

Hewitt DA, Abrecht J (1986) Limitations on the interpretation of biotite substitutions from chemical analyses of natural samples. Am Miner 71:1126–1128

Higashi J (1982) Tobelite, a new ammonium dioctahedral mica. Mineral J 11:138–146

Honma H (1996) High ammonium contents in the 3800 Ma Isua supracrustal rocks, central West Greenland. Geochim Cosmochim Acta 60:2173–2178

Honma H, Itihara Y (1981) Distribution of ammonium in minerals of metamorphic and granitic rocks. Geochim Cosmochim Acta 45:983–988

Itihara Y, Suwa K (1985) Ammonium contents of biotites from Precambrian rocks in Finland: the significance of NH_4^+ as a possible chemical fossil. Geochim Cosmochim Acta 49:145–151

Juster TC, Brown PE, Bailey SW (1987) NH_4-bearing illite in very low grade metamorphic rocks associated with coal, northeastern Pennsylvania. Am Miner 72:555–565

Livi KJT, Veblen DR, Ferry JM, Frey M (1997) Evolution of 2:1 layered silicates in low-grade metamorphosed Liassic shales of Central Switzerland. J Metam Geol 15:323–344

Massone HJ, Schreyer W (1987) Phengite geobarometry based on the limiting assemblage with K-feldspar, phlogopite, and quartz. Contrib Mineral Petrol 96:212–224

Michard A, Goffé B, Bouybaouene ML, Saddiqi O (1997) Late Hercynian-Mesozoic thinning in the Alboran domain: metamorphic data from the northern Rif, Morocco. Terra Nova 9:171–174

Mingram B, Bräuer K (2001) Ammonium concentration and nitrogen isotope composition in metasedimentary rocks from different tectonometamorphic units of the European Variscan Belt. Geochim Cosmochim Acta 65:273–287

Moine B, Guillot C, Gibert F (1994) Controls of the composition of nitrogen-rich fluids originating from reaction with graphite and ammonium-bearing biotite. Geochim Cosmochim Acta 58:5503–5523

Monié P, Torres-Roldán RL, García-Casco A (1994) Cooling and exhumation of the western Betic Cordilleras, $^{40}Ar/^{39}Ar$ thermochronological constraints on a collapsed terrane. Tectonophysics 238:353–379

Neubauer F (2002) Evolution of late Neoproterozoic to early Paleozoic tectonic elements in Central and Southeast European Alpine mountain belts: review and synthesis. Tectonophysics 352:87–103

Nieto F (2002) Characterization of coexisting NH_4- and K-micas in very low-grade metapelites. Am Miner 87:205–216

Platt JP, Vissers RLM (1989) Extensional collapse of thickened continental lithosphere: a working hypothesis for the Alboran Sea and Gibraltar Arc. Geology 17:540–543

Platt JP, Soto JI, Whitehouse MJ, Hurford AJ, Kelley SP (1998) Thermal evolution, rate of exhumation, and tectonic significance of metamorphic rocks from the floor of the Alboran Extensional Basin, western Mediterranean. Tectonics 1:671–689

Plessen B, Harlov DE, Henry D, Guidotti CV (2010) Ammonium loss and nitrogen isotopic fractionation in biotite as a function of metamorphic grade in metapelites from western Maine, USA. Geochim Cosmochim Acta 74:4759–4771

Prosser G, Spadea P, Doglioni C (1999) The high-grade basement of the Alboran Sea: structural and PT evolution. Proc Ocean Drill Program Sci Results 161:281–293

Puga E, Díaz De Federico A, Nieto JM (2002) Tectonostratigraphic subdivision and petrological characterisation of the deepest complexes of the Betic zone: a review. Geodinamica Acta 15:23–43

Ruiz Cruz MD (2008) Na-bearing white micas from Triassic rocks of the transition between Maláguide and Alpujárride Complexes (Betic Cordillera, Spain). Clays Clay Miner 56:344–358

Ruiz Cruz MD (2010) Zoned Ca-amphibole as new marker of the Alpine metamorphic evolution of phyllites from the Jubrique unit (Alpujárride Complex, Betic Cordillera, Spain). Mineral Mag 74:773–795

Ruiz Cruz (2011) Origin of atoll garnet in schists from the Alpujárride Complex (Central zone of the Betic Cordillera, Spain): implications on the P-T evolution. Mineral Petrol (in press)

Ruiz Cruz MD, Sanz de Galdeano C (2008) High-temperature ammonium white mica from the Betic Cordillera (Spain). Am Miner 93:977–987

Ruiz Cruz MD, Sanz de Galdeano C (2009a) Suhailite: a new ammonium trioctahedral mica. Am Miner 94:210–221

Ruiz Cruz MD, Sanz de Galdeano C (2009b) Exsolution microstructures in NH_4-bearing muscovite and annite in gneisses from the Torrox area, Betic Cordillera, Spain. Can Mineral 47:107–128

Ruiz Cruz MD, Sanz de Galdeano C (2010) Factors controlling the evolution of mineral assemblages and illite crystallinity in Paleozoic to Triassic sequences from the transition between Maláguide and Alpujárride complexes (Betic Cordillera, Spain): the significance of tobelite. Clays Clay Miner 58:570–584

Ruiz Cruz MD, Sanz de Galdeano C, Alvarez-Valero A, Rodríguez Ruiz MD, Novák J (2010) Pumpellyite and coexisting minerals in metapelites and veins from the Federico units in the Internal zone of the Rif, Spain. Can Mineral 48:183–203

Sadofsky SJ, Bebout GE (2000) Ammonium partitioning and nitrogen-isotope fractionation among coexisting micas during high-temperature fluid-rock interactions: examples from the New E Appalachians. Geochim Cosmochim Acta 64:2835–2849

Sanz de Galdeano C, López-Garrido AC (2003) Revisión de las unidades alpujárrides de las sierras de Tejeda, Almijara y Guájares (sector central de la Zona Interna Bética provincias de Granada y Málaga). Rev Soc Geol España 16:135–149

Schroeder PA, Ingall ED (1994) A method for the determination of nitrogen in clays, with application to the burial diagenesis of shales. J Sedim Resch A64:694–697

Schroeder PA, Mclain AA (1998) Illite-smectite and the influence of burial diagenesis on the geochemical cycling of nitrogen. Clay Miner 33:539–546

Sucha V, Kraus J, Madejová J (1994) Ammonium illite from anchimetamorphic shales associated with anthracite in the Zemplinicum of the western Carpathians. Clay Miner 29:369–377

Teppen BJ, Miller DM (2006) Hydration energy determines isovalent cation exchange selectivity by clay minerals. Soil Sci Soc Am J 70:31–40

Tubía JM, Gil-Ibarguchi I (1991) Eclogites of the Ojén nappe: a record of a subduction in the Alpujarride Complex (Betic Cordilleras, southern Spain). J Geol Soc 148:801–804

Van Zuilen MA, Mathew K, Wopenka B, Lepland A, Marti K, Arrhenius G (2005) Nitrogen and argon isotopic signatures in graphite from the 3.8-Ga-old Isua Supracrustal Belt, southern West Greenland. Geochim Cosmochim Acta 69:1241–1252

Visser D (1992) On ammonium in upper amphibolite facies cordierite-orthoamphibole-bearing rocks from Rod, Bamble Sector, south Norway. Norks Geologisk Tidsskrift 72:385–388

Vissers RLM, Platt JP, Van der Wal D (1995) Late orogenic extension of the Betic Cordillera and the Alboran Domain: a lithospheric view. Tectonics 14:786–803

Whitney DL, Evans BW (2010) Abbreviations for names of rock-forming minerals. Am Miner 95:185–187

Williams LB, Ferrel RE, Hutcheon I, Bakel AJ, Walsh MM, Krouse HR (1995) Nitrogen isotope geochemistry of organic matter and minerals during diagenesis and hydrocarbon migration. Geochim Cosmochim Acta 54:765–799

Zeck HP (1996) Betic-Rif orogeny: subduction of Mesozoic Tethys lithosphere under eastward drifting Iberia, slab detachment shortly before 22 Ma, and subsequent uplift and extensional tectonics. Tectonophysic 254:1–16

Zeck HP, Whitehouse M (1999) Hercynian, Pan-African, Proterozoic and Archean ion-microprobe zircon ages for a Betic-Rif core complex, Alpine belt, W Mediterranean—consequences for its P-T-t path. Contrib Mineral Petrol 134:134–149

Zeck HP, Whitehouse MJ (2002) Repeated age resetting in zircons from Hercynian-Alpine polymetamorphic schists (Betic-Rif tectonic belt, S. Spain). Chem Geol 182:275–292

Zeck HP, Williams IS (2001) Hercynian metamorphism in nappe core complexes of the Alpine Betic-Rif belt, Western Mediterranean-a SHRIMP zircon study. J Petrol 42:1373–1385